

VEGETATIVE AND RIVERINE SEDIMENT SOURCE CONTROLS ON AN  
EVOLVING CREVASSE SPLAY IN THE MISSISSIPPI RIVER DELTA  
A THESIS

SUBMITTED ON THE FIRST OF AUGUST 2022

TO THE DEPARTMENT OF EARTH AND ENVIRONMENTAL SCIENCES

IN PARTIAL FUFILLMENT OF THE REQUIREMENTS

OF THE SCHOOL OF SCIENCE AND ENGINEERING

OF TULANE UNVIERSITY

FOR THE DEGREE OF

MASTER OF SCIENCE

BY

Digitally signed by Katrina Ginsberg  
Date: 2022.07.29 14:45:37 -05'00'

---

Katrina Ginsberg

APPROVED: \_\_\_\_\_

DocuSigned by:

*Mead Allison*

99B09FFB9174462...

Mead Allison, PhD

DocuSigned by:

*Barbara A. Kleiss*

1441517C41744CC...

---

Barbara A. Kleiss, PhD

DocuSigned by:

*Torbjörn Törnqvist*

1A955E5CF29B469...

---

Torbjörn E. Törnqvist, PhD



## ACKNOWLEDGEMENTS

This project was funded by Louisiana's Coastal Protection and Restoration Authority through a Coastal Science Assistantship. I would like to thank my advisor Mead Allison for his guidance with this research and for all the field adventures --- I am grateful I had the opportunity to observe the fascinating and rapidly changing landscape of Fort Saint Philip. Thank you to my committee members Barb Kleiss and Tor Tornqvist --- especially Barb for her contribution of knowledge in the field and her mentorship; Ryder Myers and Kristina Leggas for assistance with the field work that made this thesis possible; and Sam Anderson for pulling me out of the mud literally and figuratively. Many thanks to my community of friends here in New Orleans who sustained interest in my progress over the years and celebrated even the small accomplishments that made up this journey. I could not have done this without your support.

## Table of Contents

Acknowledgements .....	ii
List of Tables .....	v
List of Figures .....	vi
Section 1: Introduction.....	1
Section 2: Background.....	5
2.1 Wetland Loss in Louisiana .....	5
2.2 Crevasse Splay Formation in the Mississippi River Delta .....	9
2.3 Ecogeomorphic Splay Evolution.....	13
Section 3: Study Area .....	15
3.1 Fort St. Philip Crevasse Splay Evolution .....	15
Section 4: Methods .....	18
4.1 Field Methods.....	18
4.1.1 Site Selection .....	18
4.1.2 Study Dates .....	21
4.1.3 Elevation Measurements.....	22
4.1.4 Sediment Sampling .....	22
4.1.5 Vegetation Sampling.....	24
4.2 Laboratory Analysis .....	26
4.2.1 Core Processing .....	26
4.2.2 Bulk Properties.....	27
4.2.3 Granulometry .....	27
4.2.4 Geochronological Analysis .....	28
4.3 GIS and Remote Sensing Analysis .....	28
4.3.1 Hydroperiod Analysis .....	28
4.3.2 Land Change Mapping.....	31

Section 5: Results.....	32
5.1 Mississippi River Characteristics .....	32
5.2 Hydroperiod of Study Sites .....	33
5.3 Grain Size Distributions .....	36
5.4 <sup>7</sup> Be and Feldspar Deposition .....	38
5.5 Vegetation Characteristics in Geomorphic Zones .....	41
5.6 Organic Content.....	47
Section 6: Discussion.....	49
6.1 Land Area Changes Induced by the 1973 Crevassing.....	55
6.2 Hydrologic Controls on Splay Flooding and Sediment Delivery.....	59
6.3 Vegetative Controls on Sediment Deposition .....	59
6.4 Sedimentary Evolution of the FSP Splay .....	66
Section 7: Conclusions.....	70
Section 8: References Cited.....	73
Section 9: Appendices.....	91
Appendix A: Seasonal Vegetation Survey Data .....	91
Appendix B: Seasonal Bulk Properties.....	97
Appendix C: Grain Size Statistics.....	102
Appendix D: <sup>7</sup> Be Depth of Penetration and Activities .....	104

### **List of Tables**

*Table 1.* Cores collected during each season in 2020 and 2021 at the FSP study site.

*Table 2.* List of sites and measured deposition ( $\text{cm} \pm 0.5$ ) from  $^7\text{Be}$  tracer analysis over all survey seasons. Sites are grouped by geomorphic zone and color coded.

## List of Figures

- Figure 1.* Map of south Louisiana, showing the two large sediment diversions from the MR planned by the State of Louisiana, two existing small diversions designed from salinity modification (Davis Pond and Caernarvon), and the location of the FSP crevasse splay study site. Figure modified from Swenson (2019).
- Figure 2.* Map shows early evolution of land change in the Fort St. Philip area following the crevassing event (1970-1973). Figure modified from Suir et al. (2014).
- Figure 3.* NDVI land gain (red areas) observed in Breton Sound Basin (A) between 1985 and 2005 and (B) 2009 and 2017. FSP crevasse complexed is circled in green. Modified from Potter and Amer (2020).
- Figure 4.* FSP crevasse complex area with study site circled. Map is taken from Costanza and Frank-Gilchrist (2019) and shows land growth between 2008 and 2017.
- Figure 5.* National Agriculture Imagery Program (NAIP) Aerial image of the FSP splay study area taken on October 21<sup>st</sup>, 2021 with survey sites marked. Main study sites occupied in 2021 are shown in red and July 2020 coring sites are shown in blue.
- Figure 6.* Field images of 0.2m<sup>2</sup> and 0.5 m<sup>2</sup> quadrats used for vegetation sampling at the FSP study sites.
- Figure 7.* Example of a sand/mud boundary in an extruded core that was cut to a depth of 15 cm. Arrow shows the boundary.
- Figure 8.* Study site (circled in blue) shown in relation to CRMS Site 139. The CRMS site is approximately 3,500 meters (2.2 miles) from the FSP study splay.
- Figure 9.* (A), (B), (C), and (D). Hydrographs of MR flow and turbidity at Belle Chasse for water years 2019-2021. Figure (C) shows gage height at Empire on the MR. Figure (D) shows water levels at CRMS station 139, between 11-2010 and 7-2021. Field dates at the FSP study area are shown in red (flow and stage plots include the June 2020 post-flood survey).
- Figure 10.* Seasonal water level patterns from three study sites at FSP that are representative of the geomorphic zones across the splay: Proximal, Medial and Distal. Whisker plots show minimum, maximum, mean, and interquartile range flood depths over the period of record from 2007 to 2021. Blue boxes show the Fall month (Sept-Nov), Orange shows Winter (Dec-Feb), Grey shows Spring (March-May), and Yellow Summer (June-Aug).

*Figure 11.* Hydroperiod (% time inundated) for study sites at FSP grouped by distance from the MR channel entrance plotted against their elevation (meters above MSL). Over the period of record, Distal sites towards Breton Sound are flooded to a greater depth and frequency than both Medial and Proximal sites.

*Figure 12.* FSP study area sampling sites with their measured elevation for those sites for those sites measured by RTK. Background elevations on splay obtained from USGS LiDAR data from January 2011.

*Figure 13.* Histogram of percent sand content in FSP surficial sediments at sampling sites grouped by geomorphic zone. Error bars represent the standard error of sand content of the values for multiple sites in each zone.

*Figure 14.* Depth averaged (10cm) sand fraction of each 2021 survey site grouped by distance from the MR.

*Figure 15.* (A) Grain size distribution of sand sized particles grouped by dominant vegetation growing at each site across all sampling seasons and (B) grouped by geomorphic zone. This includes all 2021 survey sites and site 25 and 29 from the June 2020 survey. Colored ranges around each lines are 96% confidence interval around the mean for each group.

*Figure 16.* Map of  $^{7}\text{Be}$  penetration depth (e.g., deposition) for cores taken immediately after the period of high MR discharge in August 2021 (red) and July 2020 (blue). Values are in cm.

*Figure 17.* Characteristic vegetation of higher elevation geomorphic zones: (A). levee site with exposed channel bank mudflat and willow in the background (Site 3, 11/7/2021); (B) monotypic *Typha* spp. stand on exposed channel bank mudflat (Site 3, 11/7/2021); typical bankline succession of *S. americanus*, *C. esculenta*, and *P. australis*, at the channel natural levee (Site 2, 8/1/2021); (C) interior zone with characteristic grasses and forbs, including *P. australis* (Site 8.5, 11/7/2021).

*Figure 18.* Field photograph of representative vegetation at lower elevation study sites in the FSP splay. (A) a patch of 2 m tall *C. esculenta* (Site 19A, 8/1/2021); (B) prograding Vegetated Mudflat showing *S. lancifolia* inland of a *C. esculenta* patch on the mudflat margin (11/8/2021); submerged Distal SAV splay with floating *P. nodosus* (Site 12, 8/1/2021).

*Figure 19.* Field photograph showing seasonal changes in vegetation characteristics. A) *P. australis* stand behind a patch of its wrack (Site 1, 11/7/2021); B) *S. lancifolia* is present in summer along with SAV in the Distal SAV sites (Site 6.5, 8/1/2021).

*Figure 20.* Solid volume fraction of vegetation grouped by dominant species that are found on the FSP splay. The submerged volume of each species was averaged across all sites where it was observed.

*Figure 21.* Averaged submerged volume fraction of vegetation grouped by geomorphic zone. Error bars show standard error among the sites comprising a zone.

*Figure 22.* Depth averaged day bulk density of soil is highest in the Proximal zone and lowest in the Medial Mudflat. These values were averaged across all seasons. Error bars show standard error between each site within a zone.

*Figure 23.* % LOI is in the surficial (0-5) centimeters. These values were averaged across all seasons. Error bars show standard error among all sites within a zone.

*Figure 24.* Percent LOI of one site representing each geomorphic zone. Error bars show standard error between each site per season. Percent LOI over the vegetation growing season varies by field site and are representative of their geomorphic zone.

*Figure 25.* Increase of land area in the vicinity of the study area between November 2006 and September 2021. Red areas show land extent in November 2006 and yellow areas additional land growth in October 2012 and September 2021. Remnant (pre-1973) marsh fringe shown in pink. Channels 1, 2 and 3 discussed in the text are labeled at their respective upcurrent entrances.

*Figure 26.* Evolution of the FSP study splay (circled) adapted from Suir et al. (2014). (A) shows pre- crevasse marsh in 1970, (B) 1978, (C) 1988, and (D) 1998. Pink circled area is the study splay and the blue circled area shows the evolution of separate wetland within the splay complex.

*Figure 27.* Interpretative map of vegetation community distributions constructed using field observations and a high resolution (2 m) drone image of the study site taken in August 2021 (Ramachandran, personal communication).

*Figure 28.* Future model projections of land change in the FSP region adapted from White et al. (2019). Maps show progressive land change in the FSP crevasse complex over 50 years under a Low RSLR scenario. FSP study splay is circled in blue.

## 1. INTRODUCTION

Artificial river sediment diversions, such as those under development by the State of Louisiana (LACPRA, 2017) in the lowermost Mississippi River (MR) are designed to mimic the natural process of crevassing, where the river channel breaches its natural levee and transports sediment-laden water into a flood basin (alluvial valley case) or a deltaic, shallow inter-distributary receiving basin (Allen, 2017). This results in the progradation and aggradation of a lobate splay deposit (Bomer et al., 2017; Wellner et al., 2005). The crevasse complex near Fort Saint Philip (FSP) is 26 km above the Head of Passes outlet to the Gulf of Mexico on the Mississippi River delta (Figure 1). It is a series of crevasse cuts that is thought to have formed when the MR breached its eastern bank during the large river flood of 1973 that continues to present in delivering river water into the adjacent Breton Sound.

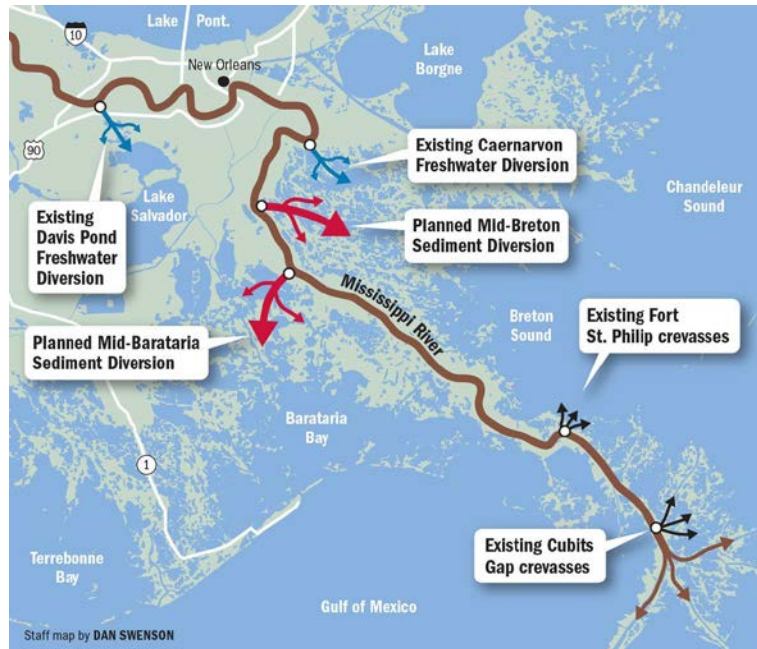


**Figure 1.** Map of South Louisiana showing the two large sediment diversions from the MR planned by the State of Louisiana, two existing small diversions designed for salinity modification (Davis Pond and Caernarvon), the Cubit's Gap subdelta crevasses, and the location of the FSP crevasse splay study site. Figure modified from Swenson (2019).

The FSP crevasse complex is comprised of a series of individual channels and cuts that exit the river, and pass through remnant marsh that was extant prior to 1973 before emerging into Breton Sound (Figure 2). As shown in Figure 2, the initial response of the receiving basin was significant erosional land loss induced by the crevasse formation.

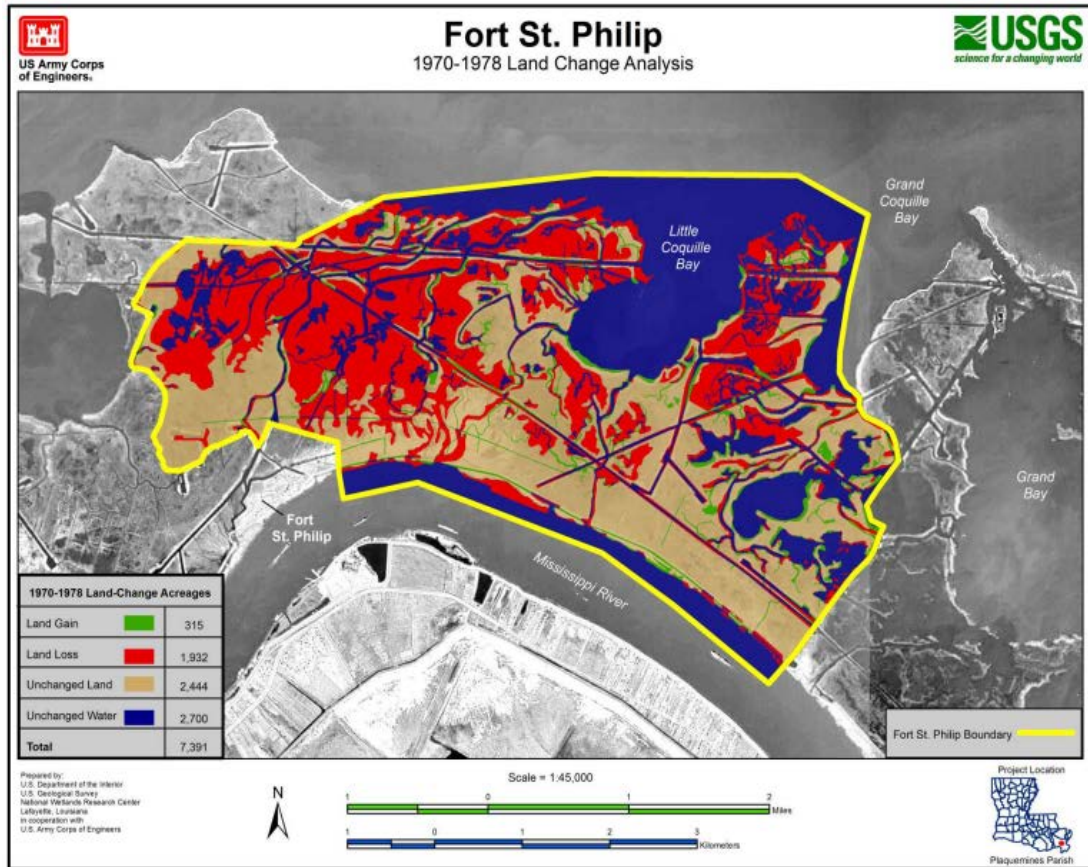


**Figure 2.** Map shows early evolution of land change in the Fort Saint Philip area following the crevassing event (1970 to 1978). Figure modified from Suir et al. (2014).

The FSP crevasses combined receive more than  $2,831 \text{ m}^3 \text{ s}^{-1}$  of MR water during maximum flow when the Bonnet Carre Spillway is open upriver, which is equivalent to about 10% of the total river flow at that discharge (Allison et al., 2012). This discharge is the same order of magnitude as the authorized Mid-Barataria and Mid-Breton diversion discharges of 50,000-75,000 cfs (1416-2124 cms) (Suir et al., 2014). The recent and rapidly evolving crevasse splay complex provides a unique opportunity to study the MR building land in the deltaic reach, by a mechanism that resembles the process before the river was heavily engineered, and is also an excellent analog to the artificial diversions that are planned upstream on the MR to build and preserve coastal wetlands in the delta.

It also provides a glimpse into the future outcome of these diversions because the crevasse has been receiving river water at this magnitude for about 50 years, which is the intended lifespan of the diversion projects for land building (Coastal Master Plan 2017).

Vegetation is a key component of wetland building that has not been robustly incorporated into numerical models used by the State of Louisiana for diversion planning (Baustian et al., 2018) despite its recognized key role in mineral sediment trapping and organic accumulation (Day et al., 2011; Fagherazzi et al., 2012; DeLaune et al., 2016; Bevington and Twilley, 2018; Larsen, 2019) . Collecting basic data (e.g. stem density and height) about vegetation communities in areas of wetland accretion in the delta is also important to inform decisions about sediment diversion planning and impacts as these parameters are known to be a primary control on mineral sediment trapping (Leonard and Luther, 1995; Mudd et al., 2010; Fauria et al., 2011; Nardin et al., 2016). There is presently a paucity of vegetation data available for evolving splays in MR deltaic situations, as well as a knowledge gap about how vegetation modifies flow and sediment trapping efficiency at the splay scale. This close association of marsh vegetation with morphologic evolution occurs both within extant marsh in the receiving basin, and, as splays become emergent, they are colonized by marsh that is likely distinct (i.e., fresher ecotype) than the extant marsh. Both types are considered in the measures of Louisiana diversion project success: area of new wetlands created and sediment trapping by extant wetlands that allows them to be sustained in the face of relative sea level rise (global + subsidence) compared to a 50 year timeline of “future without project” (CPRA Master Plan, 2017).

Without field data to calibrate flow-vegetation-sediment interactions, numerical models of splay evolution may be missing a key element that controls elevation change driven by mineral accretion through time. The objectives of this study at the FSP splay site are to 1) determine first order-controls on splay morphological evolution since the onset of growth after the 1973 flood, 2) demonstrate how patterns of sediment deposition and marsh vegetation colonization are influenced by seasonal changes in the magnitude and timing of sediment delivery (riverine and Gulf), and spatial variations in splay elevation/hydroperiod, 3) examine the impact of seasonal changes in vegetation on sediment trapping efficiency, and 4) describe how patterns of vegetation succession and community structure differ from what has been reported in the literature for other Mississippi – Atchafalaya modern crevasse splays (e.g., West Bay, Wax Lake).

## **2. BACKGROUND**

### ***2.1 Wetland Loss in Louisiana***

Louisiana contains 40% of coastal wetlands in the coterminous US and has experienced 90% of its wetland loss (Blum and Roberts 2009). These wetlands provide economic and ecosystem services exceeding \$100 billion annually (LACPRA, 2017). Engineering of the MR, including dam and levee construction in the catchment for flood control, bank stabilization, navigational improvements, and agricultural best management practices, has reduced sediment delivery overbank and into the adjacent wetlands by over 50% during the last 150 years (Blum and Roberts, 2009). Even without reduction in the MR sediment load, it is still likely that wetlands cannot maintain elevation in the face of increasing relative sea level rise (RSLR) which is presently thought to average around  $12 \pm 8 \text{ mm yr}^{-1}$  overall on the Louisiana coast, and up to  $20 \text{ mm yr}^{-1}$  in Breton Sound

region (Jankowski et al., 2017). These rates of RSLR exceed those in much of the rest of the Gulf of Mexico due to natural subsidence mechanisms such as sediment compaction and human causes such as groundwater extraction (Yuill et al., 2009). If no restoration measures are implemented to slow or reverse this wetland loss, virtually all remaining coastal wetlands in Louisiana are predicted to convert to open water by 2100, with only small areas of land gain in isolated areas surrounding the MR and Atchafalaya River outlets (LACPRA, 2017; Tornqvist 2020).

Wave erosion of wetland edges is a primary mechanism for coastal wetland loss, particularly on Gulf fronting wetlands such as in the MR Birdsfoot Delta (Wilson and Allison, 2008). During periods of high wave energy, maximum thrust is exerted onto portions of unsubmerged marsh scarp, exposing bare sediment beneath the vegetation and causing erosional scarp retreat (Fagherazzi et al., 2013). Marsh edge erosion also induces lateral shoreline retreat of interior ponds, which may have evolved from pockets of subsidence-induced interior collapse (Ortiz et al., 2017). As inland ponds increase in size due to erosion and subsidence, fetch increases across the water body, increasing wave size and energy, and thus exacerbating wave-induced edge erosion (Allison et al., 2017). Canal cutting, and their subsequent expansion through bankline collapse, is another primary driver of wetland loss, which was a widespread practice prior to the 1960's. Over 16,000 km of canals and navigation channels were dredged across Louisiana wetlands, primarily for oil and gas extraction, which fragmented wetland habitat, increased marsh edge exposure to wave attack, altered hydrologic regimes, and likely changed salinity in many places (Craig et al. 1979). Over 30km of canals were built in the Breton Sound coastal basin (Turner and McClenachan, 2018).

Hurricanes are a significant abiotic disturbance that cause coastal wetland removal in the immediate post-storm period, although the long-term impacts on marsh resilience are uncertain (Mo et al., 2020). Through multi-decadal Landsat and Modis remote sensing imagery, Mo et al. (2020) showed that intermediate and brackish marshes in the Breton Sound basin experienced a 51% and 38% decrease, respectively, in marsh area after Hurricane Katrina in 2005, mainly through a process of shearing off the organic-rich surficial substrate, although wetland edge erosion also takes place. While the marshes recovered to pre-Katrina conditions by 2008, wetland area was lost again following Hurricane Gustav later that year. Similarly, Barras (2007) used Landsat Thematic Mapper TM satellite imagery to demonstrate that hurricanes Katrina, Rita, and Gustav opened new water areas via the direct removal of wetland in fresh, intermediate, brackish, and saline marsh communities. This included the removal of post-Katrina recovery vegetation in the fresh and intermediate marshes of the upper Breton Sound (Barras, 2007).

Historical land loss rates in coastal Louisiana (Couvillion et al., 2017) measured by the US Geological Survey (USGS) are derived from aerial photographs prior to 1973, Landsat MultiSpectral Scanner data in 1973-1979, and Landsat Thematic Mapper (TM) and Landsat Operational Land Imager (OLI) satellite imagery classified into land and water categories after 1985. Couvillion et al. (2017) improved on older USGS land change algorithms by using a multi-band subtraction method called a modified Normalized Water Index (mNDWI) algorithm to enhance water features while reducing noise from land, vegetation and soil. This mNDWI is calculated from  $(\text{Green} - \text{MIR}) / (\text{Green} + \text{MIR})$ , where MIR is used because vegetation reflects more MIR light than

green light and green light reflects water. The report found a land loss rate of 7.78 km<sup>2</sup> per year in 2015 in Breton Sound basin. Amer and Potter (2020) re-examined existing remote sensing land change rates for the Breton Sound basin and reported a 24,677 ha (13%) increase of wetland area between 1985 and 2005 (pre-Katrina). USGS results from the same period showed only a 376 ha of cumulative land gain in the basin (Couvillion et al., 2011). Amer et al., (2017) developed a Normalized Difference Water Index (NDWI) for Landsat-7 Enhanced Thematic Mapper (ETM+) and Landsat-8 Operational Land Imager (OLI). This NDWI was calculated from (Blue-SWIR) / (Blue +SWIR), where SWIR is the shorter wavelength, to create land/water boundary maps at a 30m resolution (Figure 3).

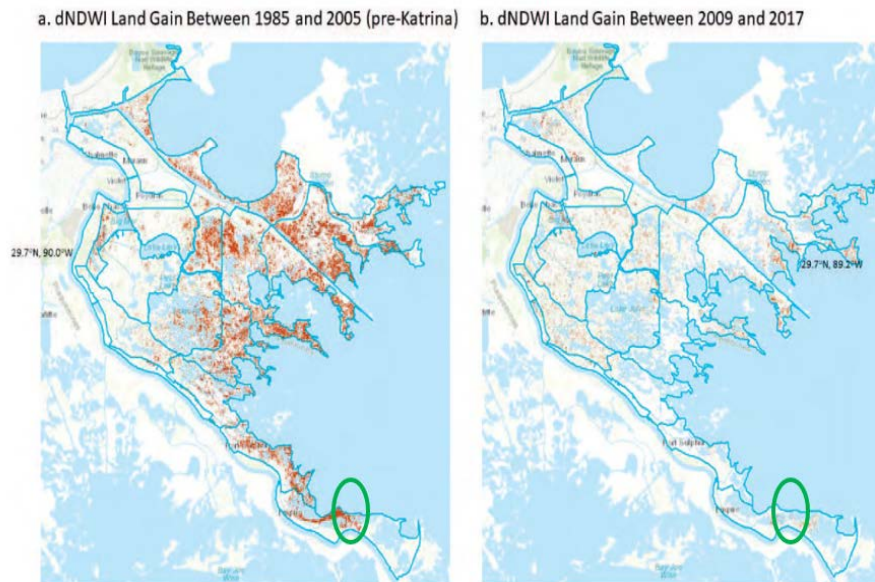


**Figure 3.** NDVI land gain (red areas) observed in Breton Sound Basin (a) between 1985 and 2005 and (b) 2009 and 2017. FSP crevasse complex circled in green. Modified from Potter and Amer (2020).

In addition, Potter and Amer (2020) combined NDWI and NDVI (Normalized Difference Vegetation Index) analysis to document gains in marshland area and green vegetation cover that occurred at a yearly rate of increase after 2008, comparable to the period between 1985 and 2005. NDVI was calculated from two Landsat surface reflectance bands using  $(\text{NIR-Red}) / (\text{NIR-Red})$ . Several previous studies have also used NDVI in Louisiana to forecast marsh collapse in the face of RSLR (Couvillion and Beck, 2013), and to examine drought-induced changes inhibiting the growth of saline marshes (Mo et al., 2017).

## ***2.2 Crevasse Splay Formation in the Mississippi River Delta***

Crevasse splays are ubiquitous features along all major Holocene distributary channels of the MR and comprise a foundational process for delta building (Wellner et al., 2005, Shen et al., 2015). In the literature, crevasse splays such as the one occurring at FSP have historically been referred to as subdeltas, which have established cyclical patterns of growth and abandonment (Coleman and Gagliano, 1964; Coleman 1988; Roberts, 1997; Wells, 1996; Wells and Coleman, 1987). These deposits are active over decadal time scales, cover only a few square kilometers in area, and generally have thin deposits <5 meters thick (Roberts, 1997). Historical average rates of subaerial growth range from 0.8 to 2.7 km<sup>2</sup>/yr (Wells and Coleman, 1987). Subdeltas are stacked upon one another, forming thick sequences in the stratigraphic record (Coleman and Gagliano, 1964). Crevasses can either persist for centuries to form splays, fill quickly with silt and heal, or erode exit channels deeply enough to capture all of the river flow, causing a complete distributary avulsion (Fisk, 1954). Crevasse splays initiate when river water breaches the river levee, and generates a turbulent jet orthogonal to the channel that is

discharged into the adjacent inter-distributary basin. Flow expands and deaccelerates, depositing sandy sediment on the basin floor at the lateral margins of the jet and forming subaqueous levees (Wellner et al., 2005). As jet momentum declines, sediments are transported downstream in suspension and as bedload to form a mouth bar, which is the subaqueous platform for major splay development. The presence of a mouth bar accelerates flow on the upstream side and slows flow on the downstream side, causing progradation (Yuill et al., 2016). After about 10-15 years of subaqueous infilling, the crevasse channel widens and increases in hydraulic efficiency so that flow bifurcates around the mouth bar into two secondary channels with an inter-distributary bay between them. These distributary channels become the conduit for delivering sediment that will rapidly build subaerial land. When splays become emergent, marsh vegetation colonizes the prograding splay and provides an additional sediment trapping mechanism (Cahoon et al., 2011). The aggrading sediment layer in the wetland colonized area is a combination of allocthonous and autocthonous organic matter and mineral sediment trapped from the riverine source by the aboveground marsh stems and leaves (Ameen et al., 2018; Larsen, 2019).

As the number of bifurcating distributary channels increases and the process expands basinward, hydraulic efficiency decreases in flow, progradation slows, and the splay vertical accretion from mineral sediment deposition declines. With reduced sediment inputs the marsh cannot keep pace with RSLR due to compaction, dewatering, wave erosion, and subsidence (Roberts, 1997). Finally the splay deteriorates and is inundated, reverting to an open bay environment and setting the stage for a renewed cycle of growth. This sedimentary cycle of infilling and abandonment is expected to last 150-

200 years (Wells, 1996). Splays are preserved in the stratigraphic record as packages of laminated fine silts and massive sands that coarsen upward, amalgamating laterally and stacking vertically (Bomer et al., 2017, Wellner et al., 2005). These facies represent the high energy building phase of the splay and are composed mainly of eroded bed material and overbank deposition (Yuill et al., 2016). The main crevasse splay facies in Holocene examples that have been studied in the MR delta are levee, distributary mouth bar, distal bar, channel, upper prodelta, interdistributary bay, and submerged marsh (Coleman and Gagliano, 1964).

Bayhead deltas like the Atchafalaya and Wax Lake deltas have a different origins than crevasse splays (e.g., river mouth versus lateral levee breaching), though the mechanisms of their geomorphic evolution are similar. These lobate (splay bar) deposits evolve as a series of arrow-shaped, mouth bar islands with the apex pointing upstream (Twilley et al., 2019). Large quantities of sand and silt are transported to a receiving basin during river floods, and build up subaqueous and subaerial natural levees that initiate subaerial emergence. The highest elevation levees are often colonized by black willow (*Salix nigra*) trees. As aggradation of the distributary mouth bars and along the levees continue, the main distributary channel bifurcates into secondary channels and extend by erosion during high flow (Shaw et al., 2013). As individual channels extend further into the receiving basin, eventually their hydraulic capacity is reduced, a levee forms across the minor distributary and cuts off that channel from sediment delivery. The abandoned channel then fills with coarse-grained distributary mouth bar and natural levee deposits, fusing into an island lobe (Hiatt and Passalacqua, 2015). A network of small secondary channels form from crevasses in the subaqueous levees, delivering sediment

from the primary distributary channels to the interior islands (Hiatt and Passalacqua, 2015).

The amount and quality of sediment retained within crevasse splays (e.g., retention efficiency) is key to effective land-building. Field data indicates that river discharge is the primary control of sediment delivery to the system, and is important for eventual sediment retention (Day et al., 2011; Allison et al., 2017; Keogh et al., 2019). Examples of active and late Holocene crevasse splays in the lower MRD that have been studied include the Brant's Pass Splay in the Cubit's Gap subdelta (active), Davis Pond Freshwater Diversion in the Barataria Basin (active), the West Bay Diversion located 4.2 km upstream of Grand Pass (active), and the Attakapas Crevasse Splay in the Lafourche subdelta (late Holocene). Esposito et al. (2017) showed that in a sheltered inland crevasse splay in the Attakapas Crevasse Splay, sediment retention efficiency ranged from 75% to 100%, with mud dominating the sediment composition. In the Davis Pond receiving area, Keogh et al. (2019) found that while the highest deposition rates occurred in Winter/Spring, the highest sediment retention was observed during the growing season Summer/Fall (81%) compared to Winter/Fall (41%). The retained sediment comprised only a third of the mineral sediment measured during Winter/Spring, suggesting that seasonal cycles of wetland vegetation density plays a key role in trapping efficiency. Retention estimates at Caernarvon Freshwater Diversion, which has a similar scale and discharge to Davis Pond, were reported as Winter/Spring (48%) and Summer/Fall (78%; Snedden et al., 2007; Koegh et al., 2019). Kolker et al. (2012) suggests that sediment retention rates for the West Bay Diversion are on the order of 30-70% depending on grain size (i.e. higher for coarser sediment).

### ***2.3 Ecogeomorphic Splay Evolution***

While the ecogeomorphology (flow-vegetation-sediment interactions) of tidal systems has been well studied, ecogeomorphic feedbacks in freshwater and intermediate wetland systems like FSP are less well understood (Ma et al., 2018). Vegetation directly alters the underlying topography via sediment trapping through enhanced settling or direct capture of sediment particles, organic matter deposition, and stabilization of substrate through root growth, which increases sediment shear strength and reduces erosion (Nyman, 2006; Mudd et al., 2009; Ma et al., 2018). Accelerated rates of aboveground plant growth lead to higher stem density, which slows water velocities across the marsh surfaces, dissipates wave energy, reduces erosion, and increases mineral sediment deposition (Lenard and Luther 1995; Christiansen, 2000; Nepf, 2012; Kirwan and Megonigal, 2013). Vegetative growth may be very important for systems that are sediment limited to maintain elevation and keep pace with sea level rise (Nyman et al., 2006). Although higher elevation results in less biomass overall due to less frequent inundation, the belowground fraction contributes biomass with an increased root to shoot ratio (Mudd et al., 2009). Both particulate organic material and mineral sediments are trapped by vegetation and gradually aggrade the marsh surface. This works in opposition to RSLR, as increased hydroperiod with rising sea levels provides more nutrients for plant growth and an increased supply of mineral sediment. Marsh collapse and conversion to open water can still occur through drowning if organic and mineral aggradation does not keep pace with RSLR (Day et al., 2011).

Controls on patterns of sediment deposition across evolving crevasse splay wetlands and deltaic islands include elevation, seasonality, and distance from the sediment source.

The elevation of marsh substrate and its effect on the frequency, depth and duration of flooding controls the development and zonation of plant communities (Cahoon et al., 2011). Deposition rates are highest in low elevation marshes that are frequently inundated for long periods of time (Temmerman et al., 2004; Cahoon et al., 2011). In the Brant's Pass Splay, variations in sediment deposition were driven by flood levels, with open water substrate showing the highest accretion rates (Cahoon et al., 2011). Seasonality impacts infrequent events like floods and storms, and the growth of vegetation. The effect of vegetation growth on sedimentation depends on the timing of that event and how tall and dense vegetation will be at that time (Nardin and Edmonds, 2014). For example, vegetation may not impact sediment deposition during winter cold front coastal setup events when it is senesced, or during summer when biomass is high but sediment delivery events are low, except for hurricanes which have been shown to produce net aggradation (Ma et al., 2018). Distance from the sediment source controls the characteristic size class of the substrate due to progressive size sorting. Sediment deposition rates are shown to decrease with increasing distance from the river entrance and marsh edge (Reed et al., 1995; Temmerman et al., 2007).

Stem density and patch size of vegetation also exert a strong control on sedimentation. In some cases, such as levees, flow has been shown to divert away from the patches of dense vegetation, reducing deposition and concentrating flow along the edges which increases erosion (Nepf, 1999; Temmerman et al., 2005, 2007; Chen et al., 2012; Nepf, 2012; Nardin and Edmonds, 2014). The reduction of sediment flux into interior islands (was observed in the WLD) in the presence of dense vegetation is described by Olliver et al. (2020) as a buffering effect. Shorter, sparser vegetation might

limit deposition through increased turbulence (Larsen 2019). It is thought that intermediate vegetation height and density enhance sediment deposition the most.

On crevasse splays and deltaic islands in coastal Louisiana, plant community distributions that are associated with specific elevation ranges undergo allogenic succession as aggradation progresses. Mature communities grow at the highest elevation and the newest communities occur at the lowest elevation. The amount of elevation change over distance controls the spatial extent of each plant community in both the along lobe and across lobe directions (Cahoon et al., 2011). An example of deltaic successional communities, in order of decreasing elevation and age, are forest, high marsh, low marsh, pre-emergent, and open water (Cahoon et al., 2011; Olliver and Edmonds, 2017).

### **3. Study Area**

#### ***3.1 Fort St. Philip Crevasse Splay Evolution***

The MR is bounded by Breton Sound on the east and provides freshwater to the basin through natural and artificial channels (Allison et al., 2012). The marshes surrounding the FSP crevasse complex are experiencing renewed sediment and freshwater delivery akin to a sediment diversion through multiple individual cuts of the complex which opened during the MR flood of 1973. Prior to the 1973 flood, the FSP complex wetlands were a vegetated natural levee with remnants of older, subsiding splay deposits (USFWS, 2003). This natural levee prevented sediment-laden river water from entering the surrounding marsh, except during high river stages with overbanking floods (USFWS, 2003). The levee breached in multiple places during the 1973 flood, incising a

series of flow channels near FSP from River Mile 24 to 16 (39 to 26 km). In 1991, the U.S. Army Corps of Engineers constructed a revetment approximately 3 km long on the east bank of the MR near FSP (USFWS, 2003). They also constructed a rock dike along the revetment length, immediately downstream of FSP. This revetment-dike system continued to allow flow through the 1973 cuts but confined their further along-river expansion of the exit points from the MR. The renewed delivery of river water through the FSP river reach since 1973 has a major impact on the extant marsh areas adjacent to the MR – this evolution has been described previously as an accelerant of land loss, due to localized marsh scour that is often associated with the initial phase of crevasse formation and marsh drowning from increased water levels (Turner, 2019), or as a natural sediment diversion that drives the building of new (splay) wetlands (Twilley et al., 2019).

Suir et al. (2014) conducted a remote sensing study of the FSP receiving area that showed significant land loss surrounding the FSP crevasse complex between 1973 and 2008, mainly through retreat of Breton Sound facing shoreline from wind and wave erosion, rather than removal of interior wetland remnants from the injection of high-velocity MR water. The report concludes that despite constant flow since 1973, the crevasse complex has been a driver of wetland loss in the area. This evidence was used by Turner (2019) to argue against the efficacy of river diversions as a restoration method for land building. During the large MR flood of 2016, a detailed measurement of water and sediment flux out of the river from the 19 largest FSP crevasses showed a total loss of 4% of the sand, 10% of the fines, and 15% of the freshwater from the MR channel (Weathers and Allison, 2016). This continuing large sediment flux has turned the receiving basin into an area of net land gain (459 ha since in the entire FSP receiving area

2008), as demonstrated by a later remote sensing study examining land change in the FSP area through 2017 (Costanza and Frank-Gilchrist, 2019). The Costanza and Frank-Gilchrist report does not include any potential land gain from the large MR floods in 2018, 2019, and 2020 when the Bonnet Carre Spillway was opened above New Orleans, and hence maximum discharge was present in the MR downstream. These three periods are maximum freshwater input events into the FSP receiving basin.

In light of the improved land change detection algorithm used by Potter and Amer (2020), the Costanza and Frank-Gilchrist report (which used older algorithms for examining satellite imagery) may have underestimated the rate of land growth at FSP. Taken together, these studies suggest that after an early phase of channel formation causing scour loss of extant wetlands, the FSP region is now transitioning to accretion, although the wetland edge adjacent to Breton Sound continues to retreat from wave impact (Suir, 2014). Given the growing evidence that the marsh surrounding the FSP crevasse complex is increasing (crevasse splays are emerging subaerially), this area presents an excellent opportunity to examine how flow and sediment from crevasse channels interact with extant wetland remnants and form new splay deposits that are colonizing by emergent and subaquatic vegetation (SAV). The trapping efficiency of MR sediment at FSP will also be impacted by the presence of the retreating marsh edge that shelters the splay area from direct exposure to Gulf of Mexico energy. This scenario provides a close analog to the proposed major goal of large artificial sediment diversions planned for the lowermost MR with the primary purpose to build and sustain wetlands.

## 4. METHODS

### 4.1 Field Methods

#### 4.1.1 Site selection

The crevasse splay study site was selected using the Costanza and Frank-Gilchrist map of land growth between 2007 and 2018 (Figure 4).

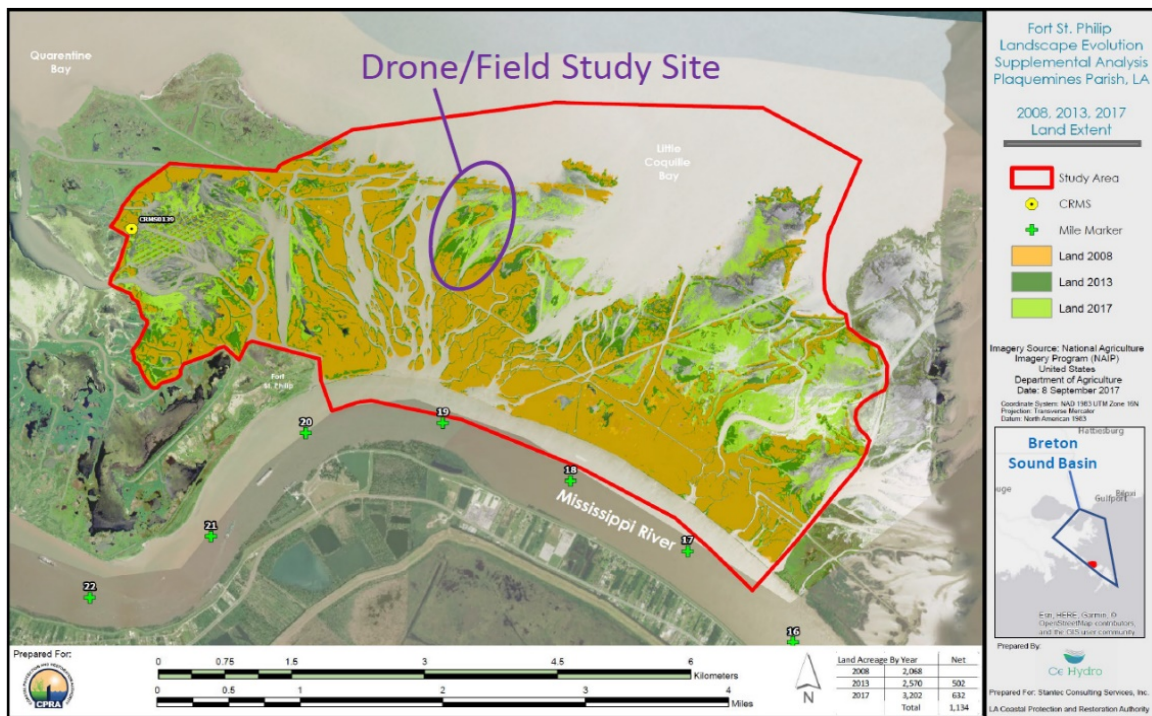


**Figure 4.** FSP crevasse complex area with study site circled. Map is taken from Costanza and Frank-Gilchrist (2019) and shows land growth between 2008 and 2017.

This site is located in the interior of the FSP crevasse complex, displays a high degree of hydrologic connectivity with the MR, remains sheltered from the Gulf by a remnant, retreating marsh edge, and shows a clear progradation of land orthogonal to the MR over

time. The splay study area measures approximately 900 m long and 200 m wide. The splay island is accessible by boat via the two crevasse channels from the MR running along either side of the splay island, and the shallow prograding mudflat at the emergent distal end accessible by pirogue. The most distal areas of the splay from the MR are intertidal mudflat only accessible at high tide either from the channels or through cuts in the eroding marsh edge bounding Breton Sound. Preliminary field sites were selected using a random stratified approach, along three longitudinal transects from the head of the splay crevasse channel to the subaqueous portion and five perpendicular transects were drawn to capture across splay variation. Preliminary site locations were situated at the nodes where these transects crossed. The crevasse splay was accessed by a Tulane University Bywater Institute boat (*R/V Shelley Meaux*). Final sites occupied were modified in the field from the preliminary grid based on accessibility on foot or by pirogue, controlled by water levels, vegetation density, and substrate cohesion (Figure 5).



**Figure 5.** National Agriculture Imagery Program (NAIP) aerial image of the FSP splay study area taken on October 21<sup>st</sup>, 2021 with survey sites marked. Main study sites occupied in 2021 are shown in red and July 2020 coring sites are shown in blue.

The 2021 survey sites were grouped by their distance from the river: Proximal (1, 7, 13); Medial (2, 8.5, 3, 19A, 19B, 4); and Distal (6.5, 12, 18) and by geomorphic zone, which includes 2020 sites: Proximal (7, 13, 21, 22), Levee (1, 2, 3, 4), Interior (8.5), Vegetated Mudflat (19A, 20, 23, 24, 27), Unvegetated Mudflat (19B, 28, 29), and Distal SAV (6.5, 12, 18, 25, 26). Elevation was an important factor in determining the geomorphic zones, but no elevation measurements were taken during the June 2020 survey. Therefore, the June 2020 sites are grouped according to spatial location, substrate quality, and dominant vegetation observed during the survey. Proximal sites from 2021 have an elevation range between 0.539-0.378 m above MSL as measured by RTK GPS rover (see Section 4.2.3) and are located at the head of the splay nearest the river, situated alongside a secondary channel connected to the main crevasse channels connected to the MR (Figure 4). Sites 21 and 22 are included in this zone because they are also adjacent to this secondary channel near the river entrance. Levee sites occupied in 2021 range from 0.454-0.295 m above MSL, and are located along the sandy natural levee adjacent the primary channel that connects the splay to the MR. Site 8.5 was the only site located in the center of the splay that was accessible for sampling. Its elevation is 0.332 m and is classified as Interior. The remaining sites are all characterized as Mudflats and are divided into three categories based on vegetation presence: Unvegetated Mudflat, Vegetated Mudflat, and Distal SAV sandflats where floating and subaquatic vegetation dominates for the summer growing season. Site 19B was the only Unvegetated Mudflat site with a measured elevation, at 0.290 m. Sites 29 and 28 were described as exposed mudflats during the June 2020 survey, and no vegetation was noted. Vegetated Mudflat sites have a lower

elevation (-0.063 m above MSL at Site 19A). They are colonized with emergent vegetation such as *Colocasia esculenta* and *Sagittaria lancifolia*. Sites 21, 23, and 24 had some floating aquatic vegetation present in the vicinity during the June 2020 survey, but were dominated by mixed emergent stands of *Typha spp.* They are located on the sheltered southeastern side of the splay, along a secondary feeder channel that does not have a direct connection to the main channel (Figure 5). Distal SAV sites are generally the furthest basinward (e.g., distal from the MR) along the prograding splay edge. They have elevations between -0.0023 and -0.199 m above MSL and receive flow from the main MR channel. These sites are dominated by the seasonal presence of floating or submerged aquatic vegetation (SAV), particularly *Potamogeton nodosus*, and are in other seasons bare mudflat or sandflat. Although sites 25 and 26 are not located as far basinward as sites 6.5, 12, and 18, they were included in this zone because of the dominance of dense floating and SAV mats observed during the June 2020 survey.

#### 4.1.2 Study Dates

Preliminary surveying and coring took place on June 16<sup>th</sup>, 2020 (Figure 5), following a prolonged MR flood year with multiple Bonnet Carre Spillway openings. This visit was also used to assess site accessibility and finalize field site selection for the main seasonal study conducted in 2021. The first of the three seasonal surveys, Winter, was conducted on March 6<sup>th</sup> and March 22<sup>nd</sup> 2021, to capture the senescent part of the vegetation growth cycle. Summer survey dates were July 31<sup>st</sup> and August 1<sup>st</sup> 2021, timed to coincide with peak vegetation growth and biomass. The final Fall survey was completed on November 7<sup>th</sup> and 8<sup>th</sup> 2021, when vegetation was beginning to senesce for the year.

#### *4.1.3 Elevation Measurements*

During the first field visit in the main study year (March 8<sup>th</sup>, 2021) elevations were measured with a Trimble R8 Real-Time Kinetic (RTK) GPS. The antenna of the RTK system received real-time correction factors via mobile internet from Louisiana State University's Center for Geoinformatics (C4G) network. The antenna was placed atop a 2 m survey pole and RTK-GPS data were collected by continuously recording position and elevation until 5 seconds of accurate data ( $\pm 3.05$  cm x, y, z location) had been collected. At each site, elevation points were recorded three times and an average elevation was calculated. The horizontal datum of the survey was Universal Transverse Mercator (UTM) Zone 16N in the North American Datum of 183 (NAD83). The vertical datum was the North American Vertical Datum of 1988 (NAVD88) and was calculated using the 2012a Geoid (Geoid12A). Vertical and horizontal units are in meters. A white PVC pole was driven into the substrate at each site where the RTK measurements were recorded to demarcate the center of the sampling region and identify the site for future visits. Locations for the coring sites occupied in 2020 (Figure 4) were determined by a handheld Garmin GPS unit.

#### *4.1.4 Sediment Sampling*

Sediment cores were collected at each site based on site accessibility during the season and depth of substrate flooding. Table 1. shows the schedule of cores collected over the entire survey. An acrylic core with a 6.67 inner tube diameter and length of between 10 cm to 20 cm, was manually inserted at a location free of vegetation but within 0.5 m to the northwest of the RTK measurement location (in the case of the 2021 study sites). The cores were sealed onsite and transported to Tulane University for lab

analysis. In March 2021 (Winter study), a 1 cm thick layer of white feldspar clay was deployed at a subset of occupied sites in a 50 x 50 cm patch where the core was collected, as a secondary method of determining sediment deposition.

**Table 1.** Cores collected during each season in 2020 and 2021 at the FSP study sites.

Cores Collected				
Site	Spring 2021	Summer 2021	Fall 2021	Summer 2020
1	x	x		
1A				
7	x	x		
13	x	x		
8.5	x			
2	x	x	x	
3	x	x	x	
19B	x	x	x	
19A	x	x		
4	x	x		
6.5	x	x	x	
12	x	x	x	
18	x	x		
21				x
22				x
23				x
24				x
25				x
26				x
27				x
28				x
29				x

#### 4.1.5 Vegetation Sampling

Vegetation was sampled at each 2021 study site using a 0.25m<sup>2</sup> quadrat made of PVC pipe for SAV sampling and a 0.5m<sup>2</sup> quadrat for land plants (Fig. 6).



**Figure 6.** Field images of 0.2m<sup>2</sup> and 0.5m<sup>2</sup> quadrats used for vegetation sampling at the FSP study sites.

The quadrat was placed within 0.5 m of the PVC central site marker over vegetation that was visually determined to represent the dominant vegetation species and characteristic distribution at that site. The quadrat was deployed twice at adjacent locations per site and an effort was made to capture the variation of the site overall. For example, one quadrat was set in a “more dense” patch and one quadrat was placed in a “less dense” patch, or one quadrat was placed in a mixed patch and another in a monotypic patch. Each plant within the quadrat was identified by species name using a report of vegetation known to occur in this splay-complex as a guide (Roy 2002). Plants on the border of the quadrat were included in the survey if the base of the stem or culm fell completely inside the plot.

Stem density was measured by counting the total number of stems per species within each quadrat, including those close to the ground, like *Alternanthera philoxeroides* (alligatorweed). Each stem height and width was measured, with average heights assigned to tall and dense monotypic stands of *Phragmites australis*. Individual leaves per stem within the quadrat were counted and measured for size with an mm-scale ruler. Percent abundance of vegetation per quadrat was visually estimated by standing over the plot and assessing stem cover versus bare substrate.

The dominant type of vegetation per site (maximum number of stems) was recorded for each site: this metric was used for analysis of submerged plant volume per season for each site to investigate how much and how often flow interacts with vegetation. Stem diameters were averaged to get a single, characteristic mean value for each plant species. Stem density was calculated as the (number of stems per plot multiplied by 2) to yield a density of each plant species per square meter. If the plant had culms that were measured (the joint at the base of a plants where multiple stems diverge), a culm density was calculated as the average number of culms multiplied by two. This “culm density” was multiplied by the average number of stems to arrive at a final stem density value. Stem widths in the field were measured near the base of the stem (e.g., within 1 to 5 cm of the substrate depending on the base height), to capture the average area that would be interacting with the flow. This was represented as a dimensionless solid volume fraction, which is defined as the fraction of underwater volume in a patch of vegetation occupied by plant matter (Wingenroth, 2019; Yang and Nepf, 2018) and

Equation 1. 
$$\frac{\% \text{ Volume Stems (cm}^3\text{)}}{\text{Total Patch Volume (cm}^3\text{)}} \times 100 =$$

$$\frac{\text{Depth of Water} \times \pi \times \text{Stem Diameter}^2 \times \text{Number of Stems per m}^2}{\text{Length of Patch} \times \text{Width of Patch} \times \text{Depth of Water}}$$

The depth of water in Equation 1. was assumed to be within 0 to 5 cm of the bed, so this value represents the volume of near bed vegetation that encounters water during most flood events.

## 4.2 Laboratory Analysis

### 4.2.1 Core Processing

Cores subsampling in the laboratory depended on the type of analysis. Cores used for radioisotope  $^7\text{Be}$  geochronology dating were vertically extruded and subsampled at 1 cm intervals for the first 5 cm, and at every other 1 cm interval to the base of the core. Cores that were not undergoing radioisotope analysis were subsampled into 5 cm combined depth intervals. Sand/mud layer boundaries and layers composed of woody or organic material were noted when cores were sectioned (Fig. 7).



**Figure 7.** Example of a sand/mud boundary in an extruded core that was cut to a depth of 15 cm. Arrow shows the boundary.

#### 4.2.2 Bulk Properties

Core subsamples were weighed to determine wet weight and then were oven dried at 60°C for a minimum of 24 hours to obtain dry weights. Water content was calculated as wet weight subtracted from dry weight. Volume of samples for bulk density calculations were standardized to 20 mm<sup>3</sup>, which corresponded to about half of the 1 cm interval subsamples. For the 5 cm samples, an aliquot of 20 mm<sup>3</sup> known volume was sectioned and removed. Saturated bulk density (SBD g cm<sup>-3</sup>) was calculated by dividing the wet weight by the 20 mm<sup>3</sup> volume. Similarly, dry bulk density was obtained by dividing the dry sample weight by aliquot volume. Porosity was calculated with the equation:

$$\text{Equation 2. } \text{Porosity} = 1 - \left( \frac{\text{SBD} - 1.01}{2.65} \right)$$

Where 1.01 g cm<sup>-3</sup> is the density of water and 2.65 g cm<sup>-3</sup> is the density of quartz, the assumed density of mineral sediment. As derived from Equation 2, porosity is a dimensionless value. Organic matter content was determined by loss on ignition (LOI) testing using the methods of Nyman (1993). Subsamples of sediment intervals from cores for LOI analysis were freeze dried to preserve the organic material and then an aliquot was combusted at 550°C for 14 hours in a furnace. LOI was calculated as the percent change in weight after combusting the freeze-dried sample.

#### 4.2.3 Granulometry

Grain size analysis was completed for every core interval of freeze dried samples that were collected during the March 2021 study trips using a Malvern Mastersizer 3000

laser diffusion scattering unit with a HydroEV dispersion system. Samples were re-hydrated with a 20 mL solution of 0.1% sodium metaphosphate overnight to deflocculate particles. Then a sediment –water solution was added to the system until a laser obscuration between 8% and 20% was reached: this obscuration is recommended by the manufacturer. Every measurement is an average of three 15 second analytical runs, one with a laser of 632.8 nm wavelength and one with a laser of 470 nm wavelength. Grain size distributions were output at 0.25  $\phi$  intervals for 0.1 to 2000 microns and statistics were a combination of those calculated internally (e.g.,  $D_{10}$ ,  $D_{50}$ ,  $D_{90}$ ) and post-calculation of other statistics (e.g., skewness, kurtosis, etc.) using GRADISTAT Version 9 software. Grain size distributions were truncated at 454 microns, to prevent coarse skewness from organic flocculates that were present in most samples. Malvern Panalytcs glass bead standards were run at regular intervals and with manufacturer recommended settings to make certain the instrument was operating within precision and accuracy limits.

#### *4.2.4 Geochronological Analysis*

A total of 18 cores (12 taken in 2021 and 6 taken in 2020) were analyzed for deposition of Beryllium-7 ( $^7\text{Be}$ ), a naturally occurring (cosmogenic) radioisotope which is adsorbed onto clay-sized particle surfaces during fallout and catchment transport (Allison et al., 2005). Given its relatively short half-life (53 d),  $^7\text{Be}$  has been used in Louisiana coastal settings as a tracer of seasonal deposition events like the impact of individual flooding: 87.5% of measured  $^7\text{Be}$  activity can be attributed to deposition from 159 days preceding coring (Keogh et al., 2019). For the present study, depth of  $^7\text{Be}$  activity was used as a proxy for the thickness of the sediment layer deposited by the MR

during that water year's flood. That is, a sample collected in the summer of 2021 would record the depositional effects of the Winter-Spring 2021 MR flood but not the 2020 or earlier floods. However, sampling and  $^7\text{Be}$  measurements late in a calendar year might also record events other than the year's MR flood such as hurricane sediment remobilization.

Aliquots of oven-dried sediment samples from the cores were ground with a mortar and pestle and packed into either vials or planar disks for analysis in three Canberra Low-Energy Germanium spectrometers. All samples were analyzed for  $^7\text{Be}$  activity for at least 24 hours. Since  $^7\text{Be}$  detection is time sensitive, all core samples were run as quickly as possible after collection and return to the laboratory, starting with the topmost interval (0-1 cm) and then moving down core until no measurable  $^7\text{Be}$  peak was observable. When multiple cores required analysis from the same study period in 2021, selected depth intervals were skipped to more rapidly arrive at a maximum depth of penetration (e.g., total deposition from the MR flood). All samples from a single core were run on the same detector (well or planar configuration).  $^7\text{Be}$  activity (dpm/g) was calculated using the net peak area of the 477 keV photopeak corrected for detector efficiency that was determined by a natural sediment standard (IAEA-Baltic Sea sediment).

### ***4.3 GIS and Remote Sensing Analysis***

#### ***4.3.1 Hydroperiod Analysis***

To determine flooding statistics (depth and frequency) for each study site on the FSP splay, hourly water levels were retrieved from the nearest Coastal Reference Monitoring Station (CRMS0139) for the entire period of record (June 2007 to July 2021) using the station's vertical datum NADV88 (Figure 8).



**Figure 8.** Study Site (circled in blue) shown in relation to CRMS Site 139. The CRMS site is approximately 3500 meters (2.2 miles) from the FSP study splay.

For each site in the FSP study area, the splay elevation measured by RTK was subtracted from the CRMS mean sea level water level to get a depth of flooding over time. The flooding depths were then grouped by season and analyzed for minimum, first quartile, median, third quartile, and maximum flooding depth values to obtain characteristic variations of seasonal flooding at various points on the splay. CRMS0139 data was determined by preliminary analysis to be more representative of water levels around the FSP splay because of its proximity to the field site: a station in the MR (USACE stage gage at Empire) and Breton Sound (USGS 07374526) were assessed but the river gage,

dominated by water level changes driven by discharge did not resemble water level changes from meteorological and astronomical tides in Breton Sound. The FSP splay can receive water from both the MR and Breton Sound.

#### *4.3.2 Land Change Mapping*

USGS LiDAR data over the study area was retrieved from the National Elevation Dataset (USGS Lidar Point Cloud [LPC] ARRA-LA\_Coastal-Z16\_2011\_000673 2014-09-17 LAS) and used to determine overall elevation trends on the FSP study area splay. The points were collected starting in January and ending in March of 2011. This is the only LiDAR image which captured the study site at a sufficiently fine scale. LiDAR points were divided into five elevation ranges based on one standard deviation ( $1 \sigma$ ) of the data. Only the ground points were used, to eliminate potential error from flooding over substrates and vegetation canopy. Ten LiDAR points at around each ground study site were averaged to obtain elevations of the splay during 2011, although some sites had no LiDAR data.

An interpretive map of vegetation community distributions on the FSP splay was drawn in ArcGIS, using a high resolution (2 m) drone image of the study site taken in August 2021 (Ramachandran, personal communication). The community distributions were determined from hundreds of geo-located photos taken across the entire FSP splay during August 2021, and ground checked by observations during field surveys. Another interpretive map of high resolution land change was created in ArcGIS using aerial historical images of the FSP complex from Suir et al. (2014) and higher resolution images focused on the study splay which were obtained from Google Earth, beginning in

1998. Images were overlain to delineate changes in vegetation/water boundaries, using site observations that were compiled during 12 visits to the study area over 3 years.

## 5. Results

### 5.1 Mississippi River Characteristics

Discharge in the MR, measured at the closest station to the FSP crevasses (USGS Belle Chasse 07374525) was an average of 14,965 cms (528,482 cfs) from October 2020 through November 2021 (Figure 9a). The MR stage at Empire (USGS Empire Waterway south of Empire, LA 07380260) reached a peak (due to storm surge moving upriver) on August 29<sup>th</sup>, 2021 (Figure 9c) with the landfall of Hurricane Ida as a Category 4 storm near Port Fourchon, Louisiana, west of the study area.

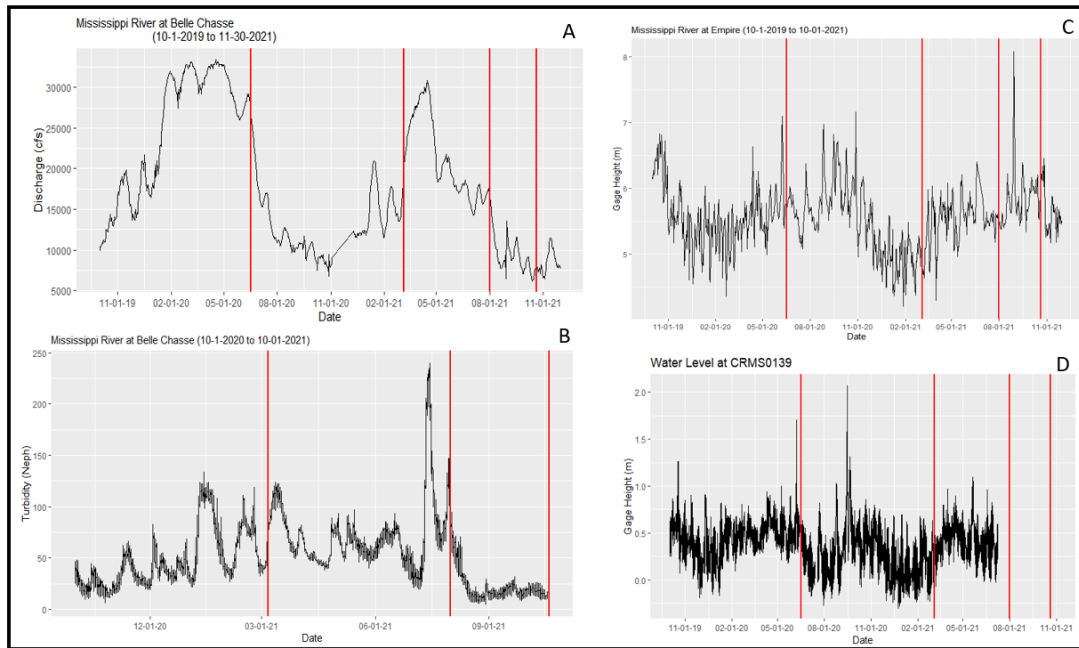


**Figure 9.** (a), (b), (c), and (d). Hydrographs of MR flow and turbidity at Belle Chasse for water years 2019-2021. Figure (c) shows gage height at Empire on the MR. Figure (d) shows water levels at CRMS station 139, between 11-2019 and 7-2021. Field dates at the FSP study area are shown in red (flow and stage plots include the June 2020 post flood survey).

Turbidity, which is a proxy for suspended sediment concentrations in the MR, generally was highest during the rising phase of discharge in the Spring of 2020 and 2021 (other than the high value during Hurricane Ida; Figure 9b.). The discharge and turbidity records at Belle Chasse show that the preliminary sampling of the FSP study area in June 2020 occurred at the end of a prolonged flood season that began in January 2020 (Figure 9a). In 2021, the three study dates corresponded with conditions of rising flow and high MR turbidity (March), falling discharge and falling turbidity (July-August), and low flow and low turbidity (November).

### *5.2 Hydroperiod of Study Sites*

As mentioned previously, hydroperiods at the study sites were calculated based on site elevation from RTK measurements and water elevation from the nearest CRMS gage. Sites generally trend to lower elevation, and, hence, increased depth and frequency of flooding, with increasing distance from the river (Fig. 10). From representative proximal (high elevation), medial and distal (low elevation) sites, Figure 10 shows that water levels in the splay area are highest in spring and lowest in winter with a seasonal variation in mean water level of about  $\pm 5$  cm.

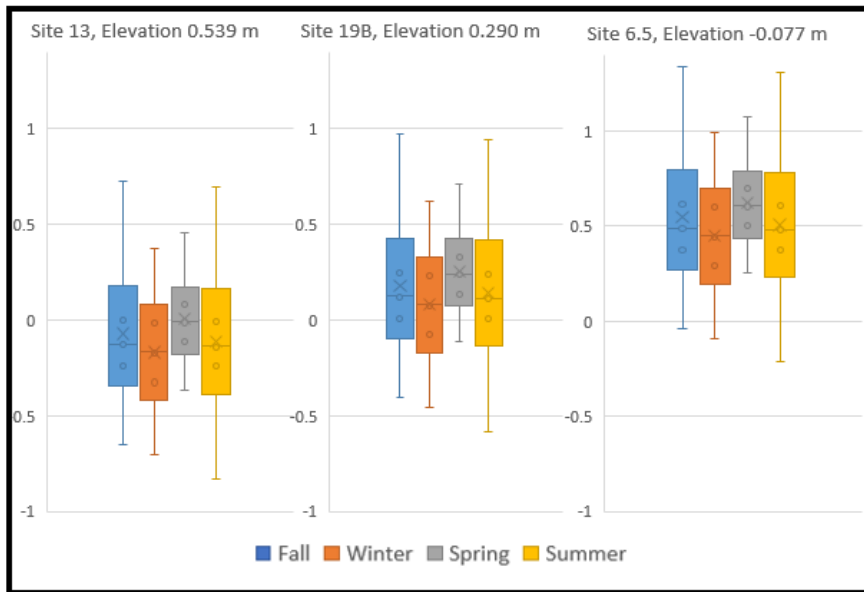


**Figure 10.** Seasonal water level patterns from three study sites at FSP that are representative of the geomorphic zones across the splay: Proximal, Medial and Distal. Whisker plots show minimum, maximum, mean, and interquartile range flood depths over the period of record from 2007 to 2021. Blue boxes show the Fall month (Sept-Nov), Orange shows Winter (Dec-Feb), Grey shows Spring (March-May), and Yellow Summer (June-Aug).

Proximal sites flooded less frequently and to a lesser depth than the Distal sites, with average depths of 37 cm distally over the 14 year record. Proximal sites do not flood on average, but have between 0.7 and 9 cm of flooding during 1<sup>st</sup> Quartile water levels over the 2007-2021 record. Medial sites are flooded to an average depth of 4 cm. Maximum flood depths were about 200 cm across the entire splay due to Hurricane Isaac on August 28<sup>th</sup>, 2012. Similarly, the water levels at the nearby MR gage south of Empire (USGS 07380260) reached a maximum of 246 cm on August 29<sup>th</sup>, 2022 during Hurricane Ida. Overall, the splay is inundated between 26 and 99% of the time, primarily controlled by

elevation related to distance from the MR mainstem (Figure 11).

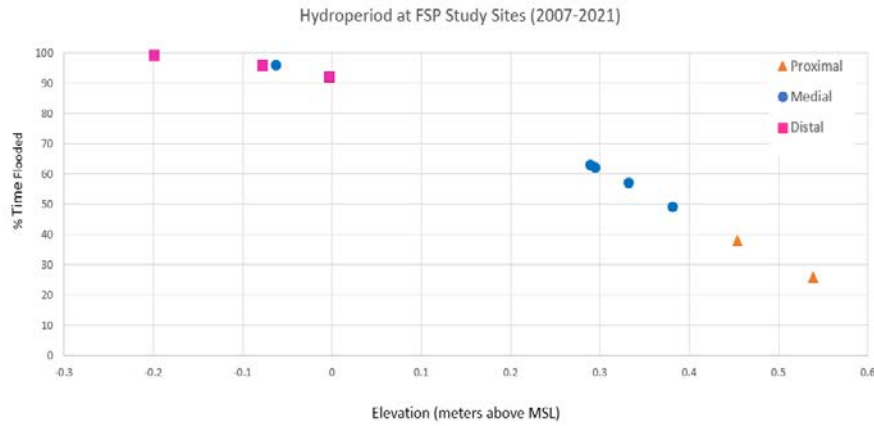


**Figure 11.** Hydroperiod (% time inundated) for study sites at FSP grouped by distance from the MR channel entrance plotted against their elevation (meters above MSL). Over the period of record, Distal sites towards Breton Sound are flooded to a greater depth and frequency than both Medial and Proximal sites.

A comparison of RTK measured splay elevations and LiDAR ground points from January 2011 shows a trend of decreasing elevation from the head (river proximal end) of the splay to Breton Sound (Fig. 12)

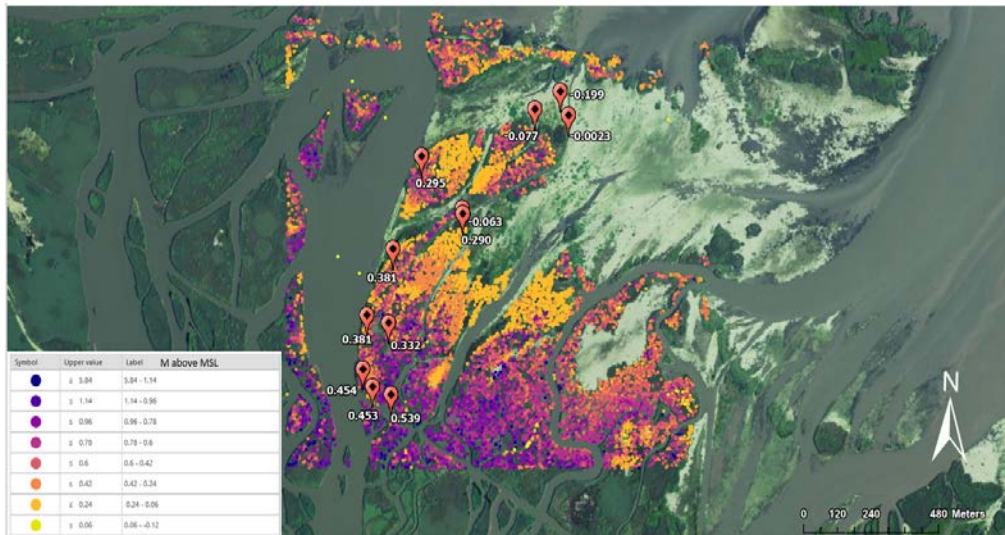


**Figure 12.** FSP study area sampling sites with their measured elevation for those sites for those sites measured by RTK. Background elevations on splay obtained from USGS LiDAR data from January 2011.

### 5.3 Grain Size Distributions

Surficial sediments integrated over the 0-10 depth interval at all of the sites had >30% sand content (Figure 13). Depth averaged sand content increases from the head of the splay to the distal region, reaching a maximum of 68% (Figure 14). Interior sites have a slightly lower sand content than channel margin levee sites. There is an increase in sand content moving from the most proximal to most distal zones (31-59%), as sand bypasses the levee and is carried by the primary crevasse channel to be deposited in the high energy distal zone.

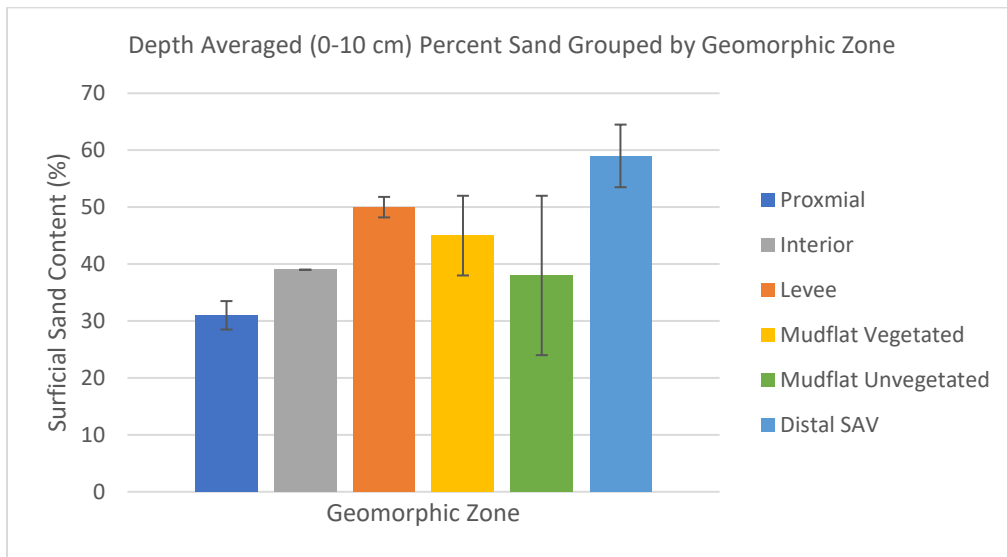


**Figure 13.** Histogram of percent sand content in FSP surficial sediments at sampling sites grouped by geomorphic zone. Error bars represent the standard error of sand content of the values for multiple sites in each zone.

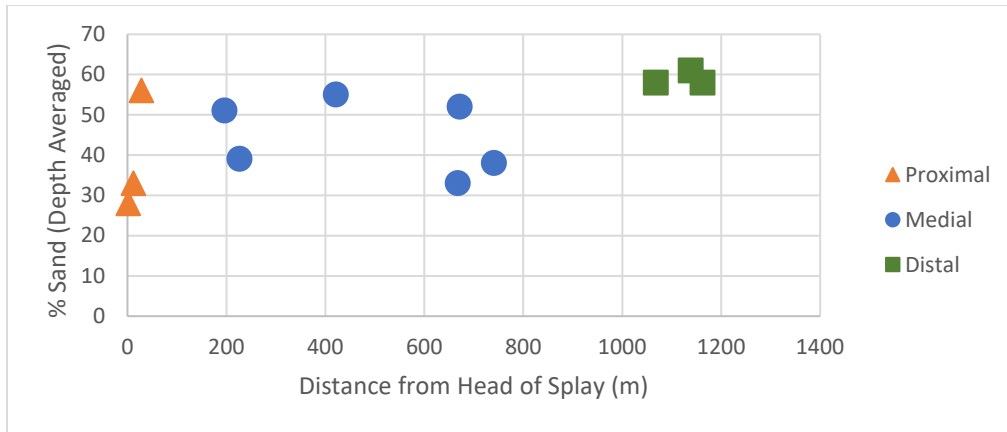


**Figure 14.** Depth averaged (10cm) sand fraction of each 2021 survey site grouped by distance from the MR.

The D50 across the entire splay ranges from 32  $\mu\text{m}$  in proximal sites to 92  $\mu\text{m}$  in distal. The grain size mixture at each study site (% clay/silt/sand) is characterized as either silty sand or sandy silt based on the primary and secondary components (Table 2 in Appendix C). Grain size distributions for all of the sites except Site 18 are skewed toward the coarse end of the distribution, reflecting the large particle organic matter that was not removed prior to grain size analysis. Surficial sediments at all of the sites can be classified as either poorly or very poorly sorted. Sites 13, 4, and 6.5 have only one mode, while the rest of the sites have up to three modes: virtually all the sites contain two prominent modes, one in the very fine to fine sand range (62.5 – 125 or 125 – 250  $\mu\text{m}$ ) and one in the medium silty (32 – 62.5  $\mu\text{m}$ ) range. Median grain size (D<sub>50</sub>) coarsens with distance from the river and with decreasing elevation. The sand fraction of % frequency grain size distributions are grouped by geomorphic zone in Figure 15A and the full grain size frequency distributions are grouped by dominant vegetation present in summer in Figure 15B.

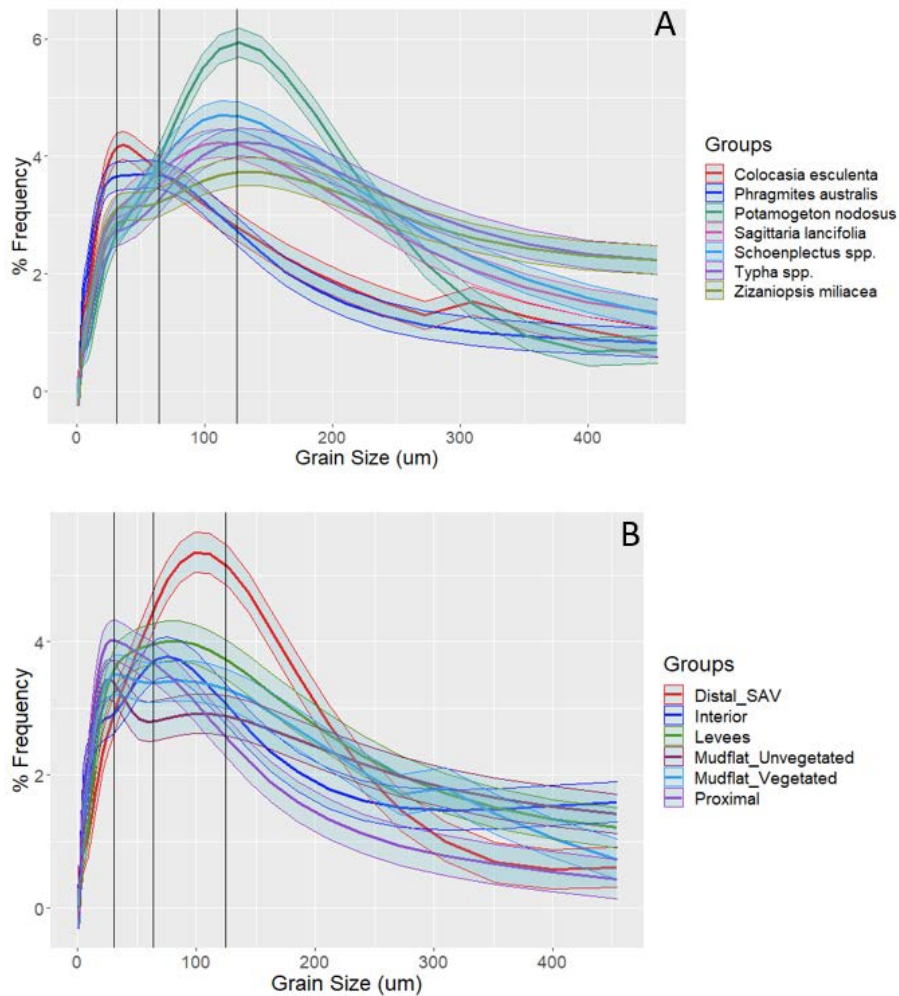


**Figure 15.** (A) Grain size distribution of sand sized particles grouped by dominant vegetation growing at the site across all sampling seasons and (B) by geomorphic zone. This includes all 2021 survey sites and sites 25 and 29 from the June 2020 survey. Colored ranges around each lines are 95% confidence intervals around the mean for each group. Vertical lines show silt, very fine sand, and fine sand size class intervals.

#### 5.4 $^{7}\text{Be}$ and Feldspar Sediment Deposition

A map of deposition across the study splay for August 2021 and June 2020 is presented in Figure 16.



of the 2020 MR flood season had significantly higher totals than those measured during any season in 2021, which is supported by the downcore  $^7\text{Be}$  activities for each site (Tables 1 through 4 in Appendix D; Figure 6). The highest deposition of all sites across all seasons was found at the Unvegetated Mudflat Site 29 with  $6.5 \pm 0.5$  cm in June 2020. Site 29 also had the highest clay content of any site surveyed at 9% (Table 3 in Appendix C). Feldspar was recovered at Sites 2 and Sites 7 during the August 2021 sampling at 6.5 cm and 4.5 cm depth, respectively. Deposition by this method was up to a centimeter greater than what was recorded for both sites from  $^7\text{Be}$  core analysis conducted at the same time.

**Table 2.** List of sites and measured deposition ( $cm \pm 0.5$ ) from  $^7Be$  tracer analysis over all survey seasons. Sites are grouped by geomorphic zone and color coded.

Site	Zone	June 2020	March 2021	August 2021	November 2021
7	Proximal	No Data	No Data	3.5	No Data
13	Proximal	No Data	0	1.5	No Data
21	Proximal	3.5	No Data	No Data	No Data
22	Proximal	2.5	No Data	No Data	No Data
8.5	Interior	No Data	No Data	No Data	No Data
1	Levee	No Data	0	0	No Data
2	Levee	No Data	0	4.5	0
3	Levee	No Data	0	0	0
4	Levee	No Data	0	0	No Data
20	Mudflat Vegetated	No Data	No Data	No Data	4.5
23	Mudflat Vegetated	6.5	No Data	No Data	No Data
24	Mudflat Vegetated	4.5	No Data	No Data	No Data
19A	Mudflat Vegetated	No Data	2.5	0	No Data
27	Mudflat Vegetated	3.5	No Data	No Data	No Data
19B	Mudflat Unvegetated	No Data	0	0	4.5
29	Mudflat Unvegetated	6.5	No Data	No Data	No Data
28	Mudflat Unvegetated	3.5	No Data	No Data	No Data
6.5	Distal SAV	No Data	0	0	0
12	Distal SAV	No Data	1.5	0	0
18	Distal SAV	No Data	0	3.5	No Data
25	Distal SAV	1.5	No Data	No Data	No Data
26	Distal SAV	1.5	No Data	No Data	No Data

### 5.5 Vegetation Characteristics in Geomorphic Zones

The dominant vegetation species observed growing on the splay at occupied study sites are elephant ear (*Colocasia esculenta*), common reed (*Phragmites australis*), bulltongue arrowhead (*Sagittaria lancifolia*), alligatorweed (*Alternanthera philoxeroides*), common rush (*Juncus effuses*), smartweed (*Polygonum* spp.), Olney's threesquare (*Schoenoplectus americanus*), giant cutgrass (*Zizaniopsis miliacea*), hairypod cowpea (*Vigna luteola*), cattail (*Typha* spp.), and maidencane (*Panicum hemitomom*).

Submerged and floating aquatic species include spike watermilfoil (*Myriophyllum spicatum*), sago pondweed (*Stuckenia pectinatus*), curly pondweed (*Potamogeton crispus*), and water stargrass (*Heteranthea dubja*) (Roy 2002).

In general, one or two species tended to dominate at a site. The distribution of vegetation communities across the splay exhibit zonation according to elevation and geomorphic zone. Willows (*Salix nigra*) grow in isolated stands on the highest areas of the channel margin levee (Figure 17a).

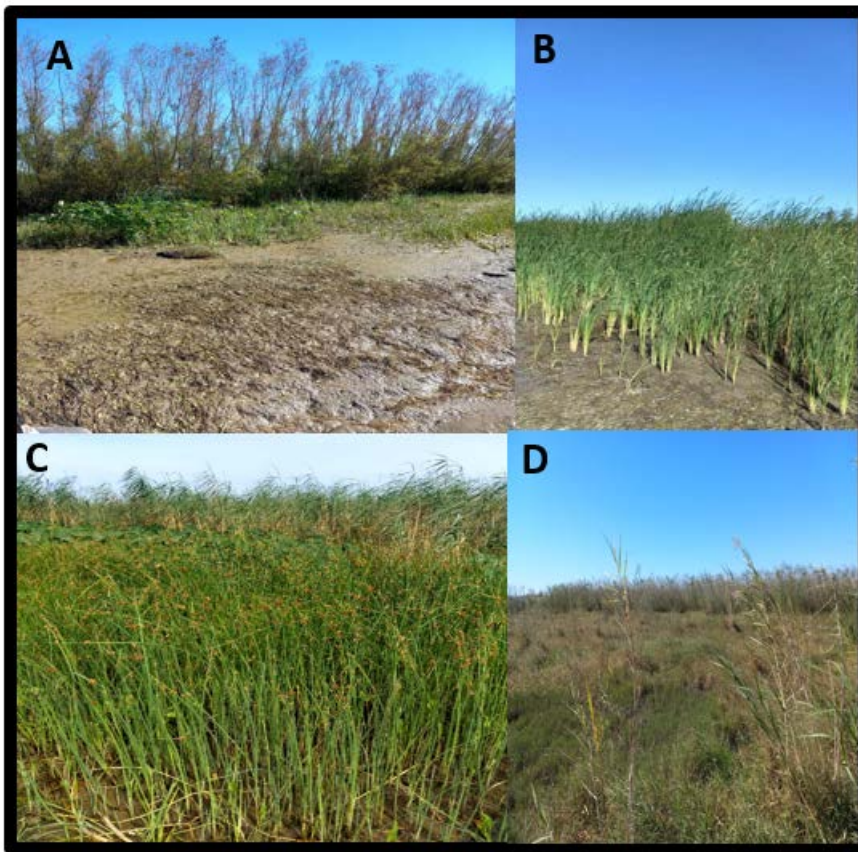


**Figure 17.** Characteristic vegetation of higher elevation geomorphic zones: (A). levee site with exposed channel bank mudflat and willow in the background (Site 3, 11/7/2021); (B) monotypic *Typha* spp. stand on exposed channel bank mudflat (Site 3, 11/7/2021); typical bankline succession of *S. americanus*, *C. esculenta*, and *P. australis*, at the channel natural levee (Site 2, 8/1/2021); (C) interior zone with characteristic grasses and forbs, including *P. australis* (Site 8.5, 11/7/2021).

They are often located on the edge of a laterally expanding mudflat along the channel bounding the splay that is periodically exposed with the tide and colonized by *Typha spp* (Figure 17b). These Levee adjacent mudflats host a typical bankline succession of *S. americanus*, *C. esculenta*, and *P. australis*, moving towards higher elevation (Figure 17c). The interior of the splay in higher elevation proximal areas is populated by grasses and forbs, with areas of interior ponding and infilling channels surrounded by *Typha spp.* and *Juncus spp.* (17d). *P. australis* is found throughout the splay but dominates at higher elevations (> 0.3 m) in the Proximal zone, the Levee zone, and the western side of the Interior zone that borders the primary channel. *Z. miliacea* occurs on the Levee zone in dense stands and is the primary species at Site 2. It is a grass with that has large, fan like culms and serrate edges. *C. esculenta* is ubiquitous across the FSP splay (Figure 18a) but favors intermediate elevations (< 0.3 m > - 0.06 m) and prograding mudflats.

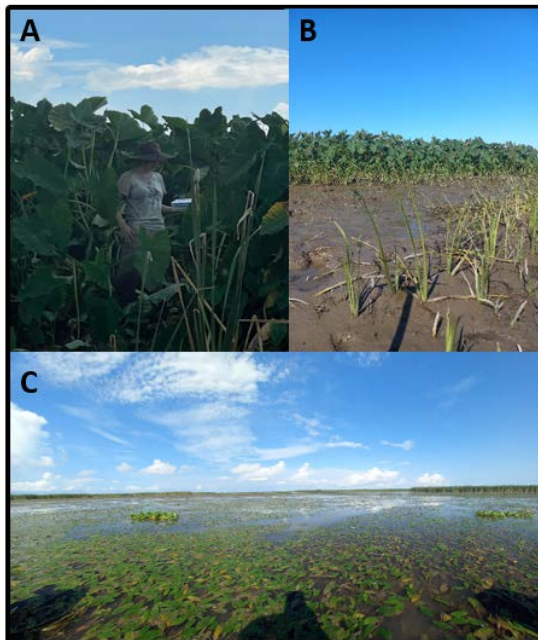


**Figure 18.** Field photograph of representative vegetation at lower elevation study sites in the FSP splay. (A) a patch of 2 m tall *C. esculenta* (Site 19A, 8/1/2021); (B) prograding Vegetated Mudflat showing *S. lancifolia* inland of a *C. esculenta* patch on the mudflat margin (11/8/2021); submerged Distal SAV splay with floating *P. nodosus* (Site 12, 8/1/2021).

*C. esculenta* co-occurs with an understory of *A. philoxeroides* and *Polygonum spp.*, interspersed among grass in the Interior, and in monotypic stands at lower elevations. It is a common early successional species in freshwater coastal wetlands in southern Louisiana that has been important contributor to land growth in both the Wax Lake and Atchafalaya deltas since those deltas were formed (Carle et al., 2015). The distal Vegetated Mudflats are populated by the pioneer species *S. lancifolia* and monotypic stands of *C. esculenta* (Figure 18b). The Distal SAV mudflats are dominated by the floating aquatic species *P. nodosus*, which anchor to the substrate via long, flexible stems (Figure 18c). Their leaves float atop the water surface and create dense mats that are coated with biofilm and layers of sediment. These floating aquatics were observed to be present only from July through September during the field visits.

Vegetation growth across the splay displays a strong seasonal component. Vegetation size was significantly more robust in August. A dramatic example of this is the interior site 19A, where *C. esculenta* that measured 30 cm tall in March with a density of 24 stems per square meter, grew to a height of nearly 2 meters tall in August with double the stem density (Table 1 in Appendix A). The quality of vegetation also shifts. For example, *P. australis* is characterized by tall, nearly impenetrable monotypic stands in summer and sparser stands in winter that form expansive areas wrack following floods and senescence (Figure 19a). Certain vegetation is only present seasonally, like the floating and SAV on the Distal mudflats. In August, Site 6.5 showed sparse patches of

emergent *S. lancifolia* growing among the floating aquatics that was not present during other seasons (Figure 19b).

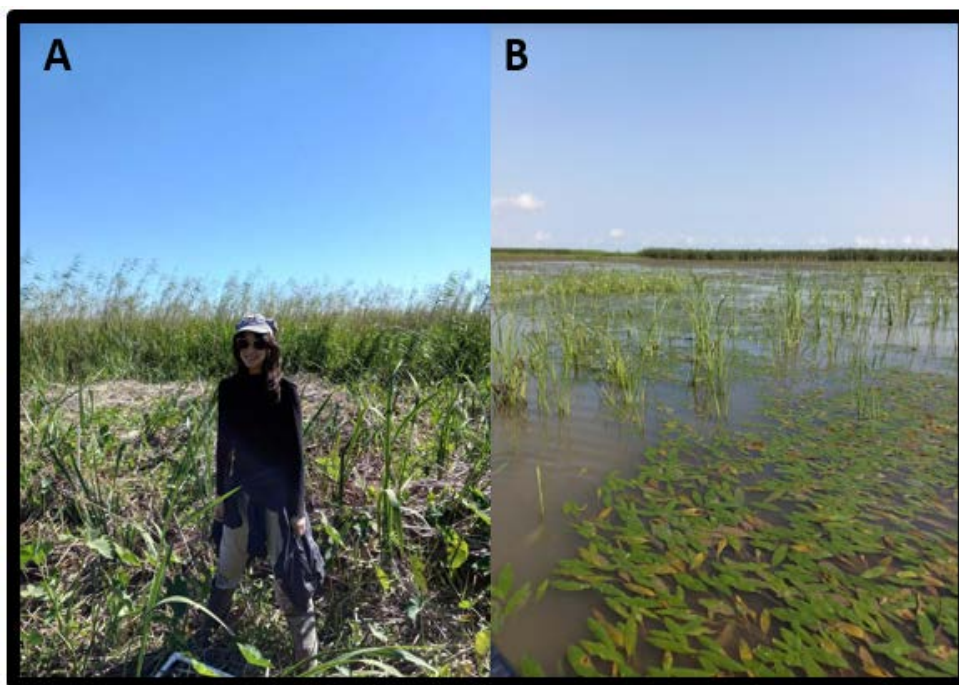


**Figure 19.** Field photograph showing seasonal changes in vegetation characteristics. A) *P. australis* stand behind a patch of its wrack (Site 1, 11/7/2021); B) *S. lancifolia* is present in summer along with SAV in the Distal SAV sites (Site 6.5, 8/1/2021).

Vegetation resistance to flow is dependent on its depth of submergence, which varies with hydroperiod. Figure 20 shows seasonal changes in the average submerged fraction of vegetation for the dominant species at each of the sites (see section 4.1.5 for calculation method). The volume of vegetation interacting with flow is highest in August, followed by November, and then March (Figure 20).

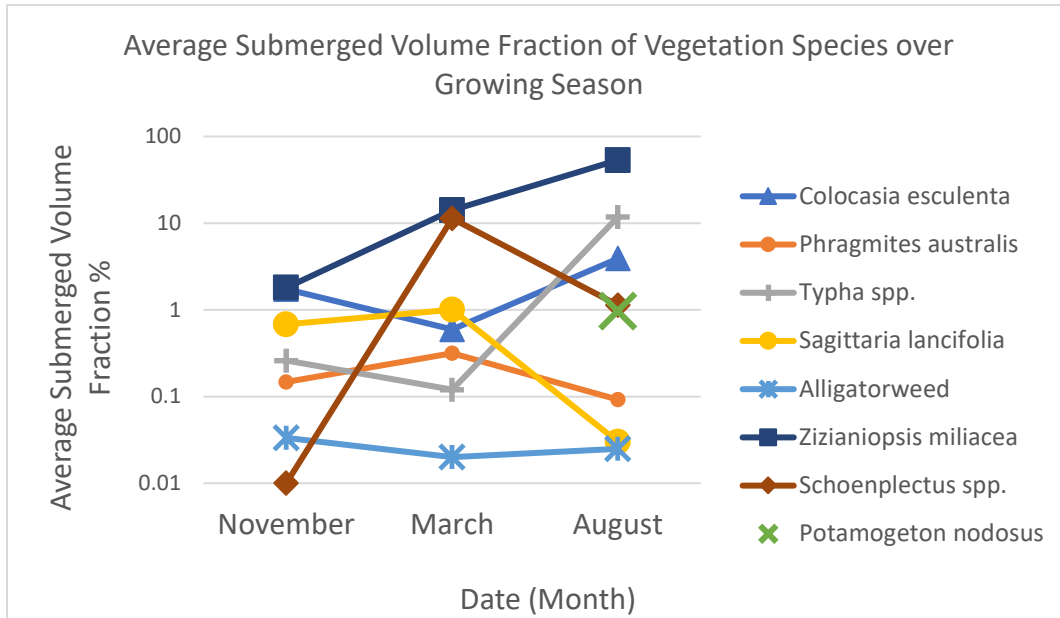


**Figure 20.** Solid volume fraction of vegetation grouped by dominant species that are found on the FSP splay. The submerged volume of each species was average across all sites where it was observed.

Only *Z. miliacea* increases its fractional volume of biomass encountering flow over the typical growing season between November (senescence) and August (peak biomass). *C. esculenta* and *Typha spp.* have the lowest solid volume fraction in March, followed by a spike in growth during the August measurements. *S. lancifolia*, *P. australis*, and *Schoenplectus spp.*, reached peak growth in March, and decline in fractional volume by August. Submerged volume increases with increasing elevation and D50 during August. However, there is no strong relationship between D50 and stem density across all seasons. Stem densities generally increase from March, reach a peak in August, and then decline by November (Table 2 in Appendix A). This pattern does not hold for Site 7, which is dominated by *P. australis* that shows peak growth in March (Table 3 in Appendix A). Figure 21 shows solid volume fraction grouped by geomorphic zone and

reveals that the Levee zone has the highest value ( $4.4\% \pm 1.4$ ), followed by Vegetated Mudflat ( $1.1\% \pm 0.4$ ). The rest of the zones average between 0.08% and 0.13 %.

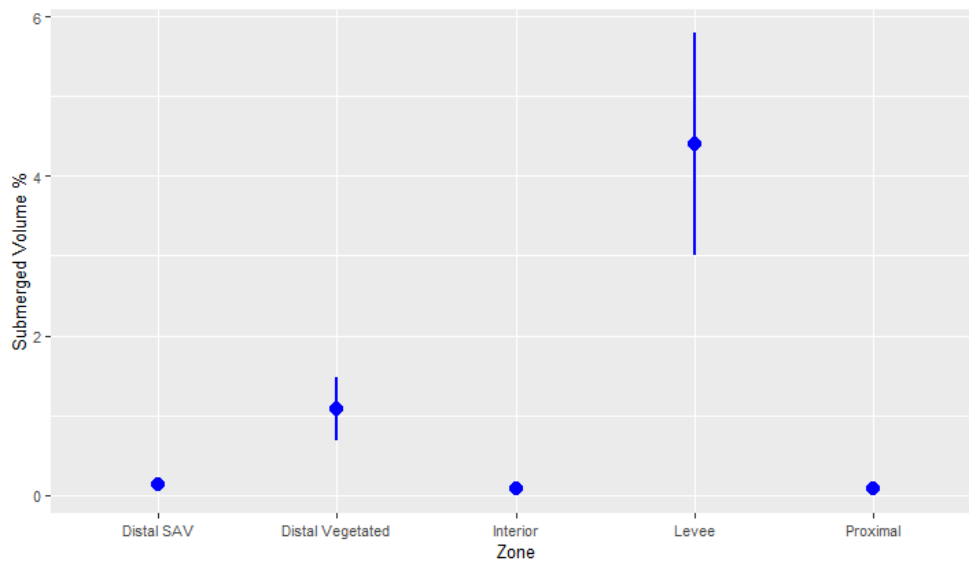


**Figure 21.** Averaged submerged volume fraction of vegetation grouped by geomorphic zone. Error bars show standard error among the sites comprising a zone.

## 5.6 Organic Content

In the surficial centimeters (0-10 cm depth), coastal wetland sediments usually have very low bulk densities, within the range of  $0.1\text{-}0.6\text{ g cm}^{-3}$  (Nyman et al., 2006; Keogh et al., 2019; Twilley et al., 2019). Bulk density estimates on the FSP splay in the proximal and levee zones approach values found at  $>2$  m depth in MR sediments, at  $1.5\text{--}1.2\text{ g cm}^{-3}$ , respectively (Keogh, 2021; Figure 22). Bulk density decreases moving towards Breton Sound and the Distal SAV sites average  $0.6 (\pm 0.03)\text{ g cm}^{-3}$ . Organic content for the FSP splay is relatively low compared to other peat rich freshwater marshes in the region, which have between 20-32% organic content on average and up to 75% for true peat (Allison and Wilson, 2008; Sapkota and White, 2019). Average %LOI values ranged from  $6.4\% \pm 0.73$  (Distal) to a maximum of 23% (Interior) (Figure 23).

LOI values varied seasonally by site and thus dominant vegetation species. Sites 19B and 3 showed peak LOI values in March, while site 2 peaked in November and 12 and 6 showed maximum values in August (Figure 24). Organic content decreases with increasing distance from the MR entrance. LOI does not appear to have a relationship with grain size.

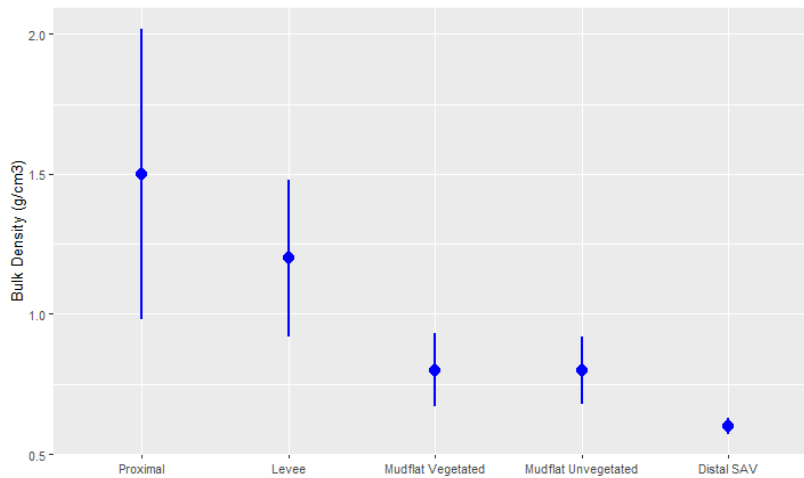


**Figure 22.** Depth averaged day bulk density of soil is highest in the Proximal zone and lowest in the Medial Mudflat. These values were averaged across all seasons. Error bars show standard error between each site within a zone.

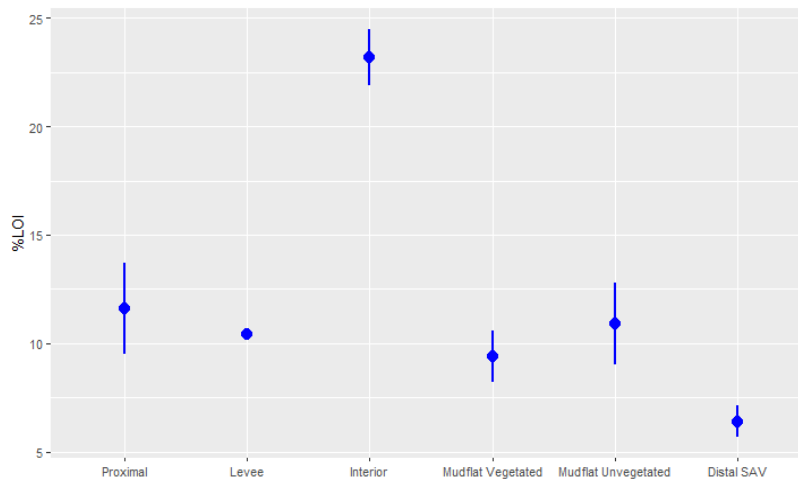


**Figure 23.** % LOI is highest in the surficial (0-5) centimeters of the Interior, followed by the Proximal and Levee zones, respectively. These values were averaged across all seasons. Error bars show standard error among all sites within a zone.

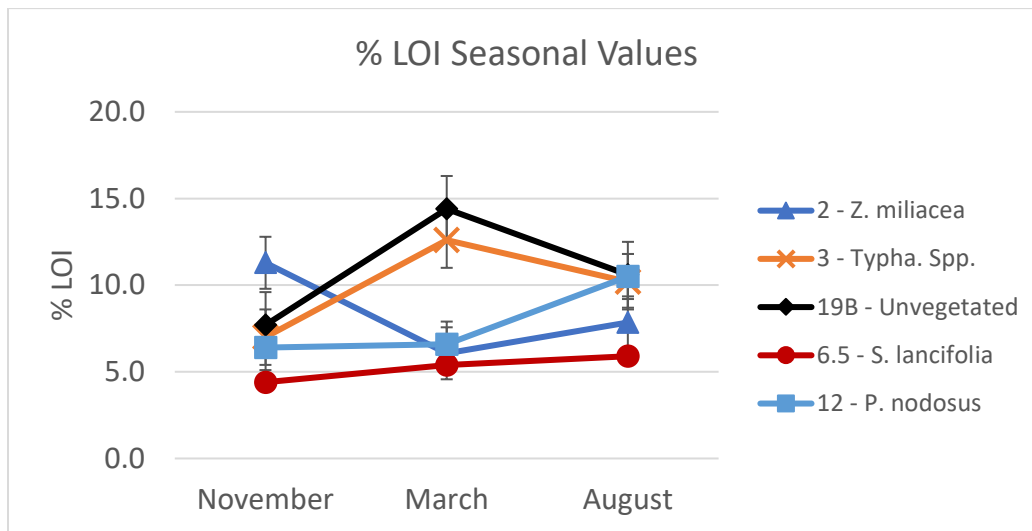


**Figure 24.** Percent LOI of one site which hosts a distinct monotypic vegetation species. Site 2 is *Z. miliacea*, 3 is *Typha spp.*, 19B is unvegetated, 6.5 is *S. lancifolia*, and 12 is *P. nodosus*. Error bars show standard error between each site per season. Percent LOI over the vegetation growing season varies by field site and are representative of their geomorphic zone

## 6. DISCUSSION

### 6.1 Land Area Changes Induced by the 1973 Crevassing

In the time following the crevassing events during the 1973 MR flood, sections of the FSP splay located within the remnant marsh belt between the MR and Breton Sound, including the study site, have increased in wetland area overall, particularly since 2006 (Figure 25).

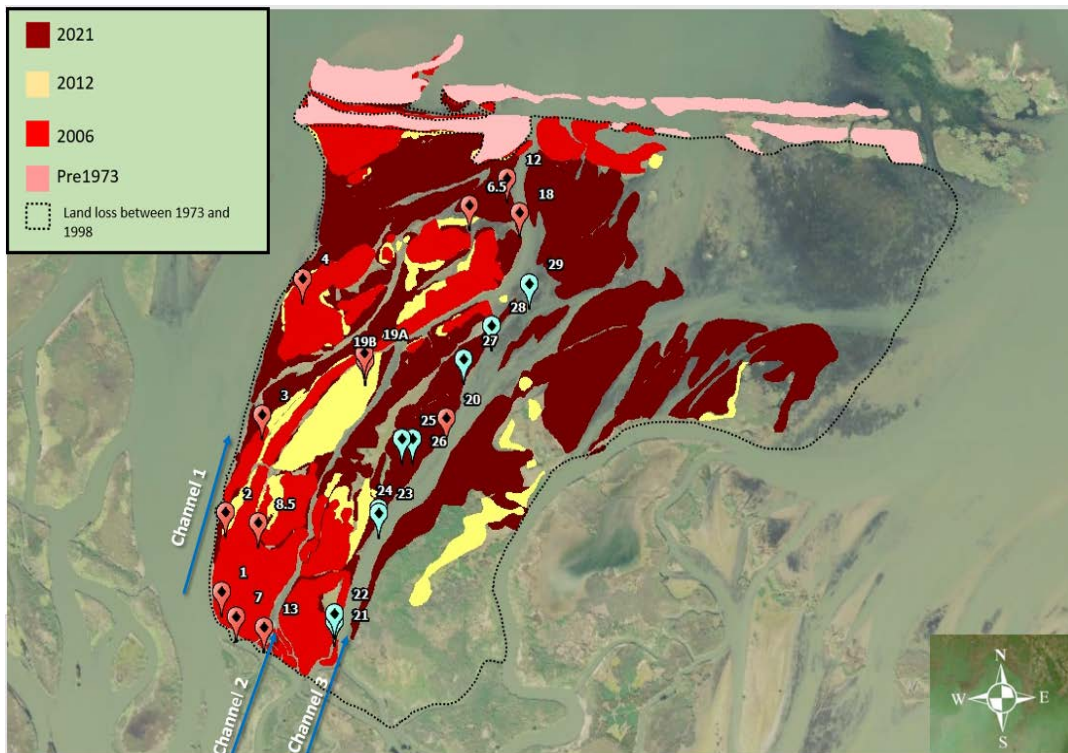


**Figure 25.** Increase of land area in the vicinity of the study area between November 2006 and September 2021. Red areas show land extent in November 2006 and yellow areas additional land growth in October 2012 and September 2021. Remnant (pre-1973) marsh fringe shown in pink. Channels 1, 2 and 3 discussed in the text are labeled at their respective upcurrent entrances.

Remote sensing images of the entire splay complex before the 1973 crevassing events show an area of contiguous marsh (Figure 26A). After the crevassing event, the proximal marsh was eroded away (Figure 26B). Suir et al. (2014) quantify this period (1970-1978) as resulting in over 7.8 km<sup>2</sup> of net land loss within the entire FSP region. Overall, the years between 1973 and 1998 were of net land loss, likely due to a combination of the onset of high-velocity channelized flows from the MR acting on remnant wetland in the belt between the MR and Breton Sound, and subsidence in the region. Figure 26 shows a

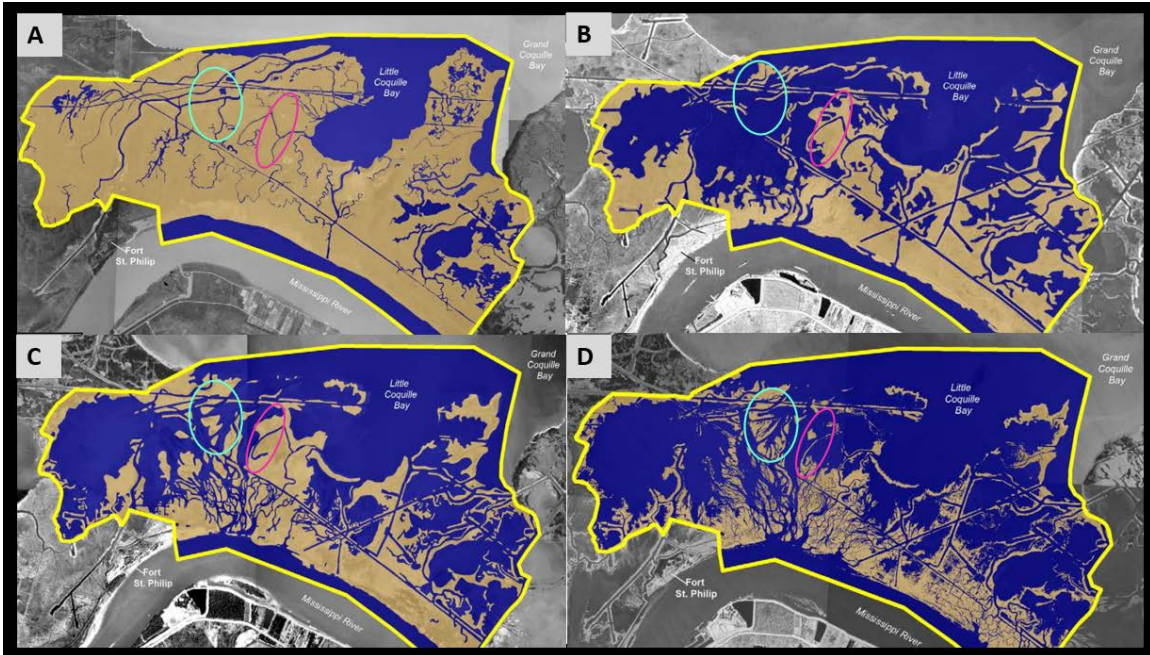


**Figure 26.** Evolution of the FSP study splay (circled) adapted from Suir et al. (2014). (A) shows pre-crevasse marsh in 1970, (B) 1978, (C) 1988, and (D) 1998. Pink circled area is the study splay and the blue circled area shows the evolution of separate wetland within the splay complex.

separate splay region to the west of the study splay, which appears to have completely eroded after the crevassing, and infilled to its present marsh configuration by 1998. In the Costanza and Frank – Gilchrist report, this area appears as unchanged land on the opposite side of the primary crevasse channel to the study splay. It is reasonable to conclude that this crevasse complex is a dynamic site for wetland growth.

The first aerial images of the study splay at a sufficient resolution to precisely identify land/water boundaries were taken in 1998 by Landsat Copernicus, published by the USGS, and analyzed in the present study via Google Earth historical imagery. There appears to be no significant change in land/water boundaries on the study area splay between 1998 and 2006 from the higher resolution (~10 m/pixel) imagery. Suir et al.'s

analysis only quantify the larger FSP area as net depositional beginning in 2008, but edge retreat of the remnant marsh boundary fronting Breton Sound continued apace, partly counterbalancing the land area growth numbers, but also continuing to serve as a shelter for splay growth in the study area. Most of the pre- crevasse remnant marsh, besides the most basinward fringe, has since eroded and forms an area of new accretion (Figure 25). Costanza and Frank-Gilchrist's later analysis (2019) showed that the entire FSP area has undergone a net gain of 459 ha since 2008. Sediment delivery and infilling has accelerated since 2008, and includes a period marked by maximum MR floods when the Bonnet Carre Spillway was open upriver in 2008, 2011, 2016, 2018, 2019, and 2020. The analysis of Google Earth imagery in Figure 26 shows that the study splay and the area immediately surrounding it has created an estimated 51 ha of wetlands since 2006. This includes 7.5 ha of growth between 2006 and 2012, and 43 ha between 2012 and 2021. Land/water boundaries for the Google Earth analysis were delineated by vegetation boundaries spot checked during visits to the FSP splay. Although this method is not nearly as sophisticated or accurate as Potter and Amer's (2020) methods of combining NDVI with NDWI metrics, it does support their conclusion (and Suir and Costanza and Frank-Gilchrist's) that marsh area is increasing at an accelerating pace relative to the period between 1985 and 2008 in the FSP study reach.

The directionality of the observed progradation in the study area between the MR and the remnant marsh fronting Breton Sound is indicative of sediment sourcing from the MR. Progradation has likely been aided via protection of the evolving splay from Gulf wetland edge (wave) erosive processes (Wilson and Allison, 2008) by the remnant marsh edge on the seaward side. The erosive effect has continued to cause this remnant edge to

retreat at an estimated rate of 11 – 22 m/y since 1973 (Suir et al., 2014; Figure 25). The highest elevation in the study area occurs on the head of the splay, proximal to the MR (Figure 12). This proximal zone is the oldest part of the splay and was present as remnant marsh prior the crevasse breach in 1973 (Figure 2). While most of this proximal marsh appears to have been eroded during the initial crevassing event (Suir et al., 2014), the remnant marsh fragments likely formed the nucleus for initiation of the present phase of splay growth. The erosion of remnant wetland area may have planed off the substrate surface and deposited an armoring sand layer that became the basis for later aggradation, while limiting further downcutting.

The FSP study splay shows land growth orthogonal to the MR since 2008 (Costanza and Frank – Gilchrist, 2008) which was a major reason it was selected for the present analyses. The combination of erosion and subsidence described above created accommodation space for a renewed cycle of wetland growth. However, a similar splay directly to the west of the study splay, does not show this same reduction in wetland area over time (Figure 26).

## ***6.2 Hydrologic Controls on Splay Flooding and Sediment Delivery***

The opening of multiple MR crevasses in the FSP reach in 1973 resulted in a series of anastomosing channels that cross a 2,190 m wide belt of remnant wetlands before emerging into Breton Sound. This pattern of channelization has infilled the shallow (generally less than 1.5 m deep) open water areas between the wetland remnants with splays after an initial erosion phase outlined in 6.1. The location of primary (connected to the MR) and secondary channels that branch off them in this complex has also likely been a primary control on sediment supply to splay areas. In the case of the

study area splay, this has meant formation of only one well-developed natural levee instead of two natural levees on either side of the arrowhead islands: a pattern that characterizes the well-documented bayhead deltas of the Mississippi-Atchafalaya (Shaw et al., 2013). Channel 1 in Figure 25 is likely a direct conduit for delivering coarse riverine sediment to the natural levee via unidirectional flow. While LiDAR observations do not resolve small-scale differences in elevation (Figure 12), field observations suggest the natural levee opposite Channel 1 is higher in elevation than the channel margins that line secondary Channels 2 and 3. The Channel 1 levee is up to 51 cm higher than the distal mudflats, particularly those at the prograding region on the opposite (eastern) side of the splay that receives water and sediment through secondary channels sourced from this larger channel. Instead of an open interdistributary bay that gradually slopes towards a lower elevation seaward to the Gulf, as is the setting of the Wax Lake bayhead delta, the subtidal middle portion of the FSP study splay has subaerial mudflats that are rapidly infilling behind the Gulf-fronting remnant fringe. The Mudflat sites from the 2021 survey are bounded by a narrow channel with incised (erosional) banklines approximately 2 meters deep (Channel 2, Figure 25). Reversing tidal flows were observed in these secondary channels, unlike Channel 1 where flow is always seaward due to the MR outflow.

Hydroperiod of a specific site on the FSP study splay is first-order controlled by elevation: higher elevation proximal and natural levee zones flood only during events lasting hours to several days, while the distal end of the splay and adjacent vegetated and unvegetated flats below mean tide flood diurnally. Flooding the higher points on the splay requires the convergence of a specific set of conditions so that water levels are high

enough to overbank the channel margin levees and penetrate into the interior. These conditions are favored by (1) onshore winds/coastal setup, (2) summer thermal expansion of the Gulf, (3) high astronomical tide, and, to a lesser extent, (4) high MR stage.

Flooding of the FSP study area splay with turbid MR water is highly episodic in all seasons. The complexity of the sources for high water events on the splay mean that either the MR or the Gulf can serve as the source of water for flooding, with likely differences in the turbidity and grain size of the sediment advected to the splay. While water levels at the nearest CRMS sites are broadly linked to MR stage (Figure 9C and 9D), the CRMS record is marked by episodic high and low water events that do not align with MR discharge and are of meteorological origin. Tidal processes contribute to high water episodes on the splay, with spring tide occasionally reaching  $\pm 30\text{-}40$  cm MSL. Gulf water levels are highest overall in the summer and fall season due to thermal expansion, but can be super-elevated for several days at a time due to strong pre-frontal onshore winds during the cold front season (October –April) or from tropical storms in late summer and fall. The river's timing is more important for the suspended sediment concentration in water delivered to the study area. MR suspended sediment loads are elevated in the December-June period, generally in one or more flood events lasting for weeks to several months. MR basin hysteresis impacts inundation timing and sediment delivery because rising hydrograph conditions in the MR generally are more sediment charged than the high-to-falling limb conditions (Allison et al., 2014). Given that geochronology methods ( $^7\text{Be}$ ) used in the present study cannot resolve the impact of individual flooding events of distinct suspended sediment concentration and grain size, in

the future, high temporal-frequency monitoring will be needed to determine the impact of individual high water events on sediment supply to the splays.

The higher deposition rates observed on the FSP splay in June 2020 versus the 2021 studies also suggests that MR flood magnitude and duration, hence total sediment load delivered through the crevasses, plays major a role. Both 2020 and 2021 reached peak flow (measured by operation of the Bonnet Carre Spillway upriver), but the flood of 2020 lasted from February through June, while the 2021 event was of much shorter duration (March-April; Figure 7). Not only was 2020 deposition of a greater magnitude on the splay, but  $^7\text{Be}$  activities (dpm/g) were higher (indicative of particles that were river sourced; Galler and Allison, 2008) compared to the 2021 core results (see Figure 2 in Appendix B).

March was the only field study visit in which flood water was observed on the portion of the splay above mean high tide and it was only on the order of a few centimeters, not substantial enough to record flow velocities. The March visit coincided with the rising limb of the 2021 MR spring flood and corresponding spike in river turbidity (Figure 9C), yet almost no deposition was observed in  $^7\text{Be}$  sediment cores from the splay. This is interpreted to mean that despite MR sediment source being high, flooding of the splay was infrequent during the Winter-Spring period due to low Gulf level (cold) and significant sediment did not reach the higher points on the splay. Conversely, the August visit occurred during the falling limb of the spring MR flood, after the waters had receded. Most of the  $^7\text{Be}$  deposition in this study was recorded during August 2021, indicating the integrated effect of significant flooding and deposition events during the time interval between March and August. This window of time coincided with

peak MR discharge (Figure 9A), with a warming Gulf, and with episodic late spring frontal events that caused strong pre-frontal setup events that lasted up to several days.  $^7\text{Be}$  deposition measured in cores from the splay remained high in November of 2021 study. This may be a result of the passage of Hurricane Ida to the west of the field area in late August, as this event inundated the entire splay: a storm surge of up to 8 m was recorded in the MR stage gages opposite the field area (Figure 9C).  $^7\text{Be}$  from the spring flood would be approximately two half-lives ( $^7\text{Be} = 53\text{d}$ ) old, and thus at ~25% of their activity at the time of deposition. This implies that  $^7\text{Be}$  found in November cores was mainly due to new sediment brought to the marsh surface by the storm, potentially sourced from the river surge and/or from large waves reworking the inner shelf and marsh edge deposits. During the November field study, no significant marsh damage was observed on the FSP splay, suggesting little erosional impact from the surge and Gulf waves.

Coring surveys in 2020 and 2021 also indicated there is significant spatial variability in deposition across the splay that is likely linked to hydroperiod as well as spatial variations in sediment load carried into the area by primary and secondary channels outlined above. Hydroperiod here is defined as frequency of inundation with turbid river water.  $^7\text{Be}$  deposition in the 2021 flood on the western splay levee ranged from 0 to 4.5 cm (Figure 14), suggesting that the relatively high elevation leads to irregular overbanking along lower sections of the levee and into the splay interior. There is limited information on sedimentation in the proximal half of the interior as only one site was measured for  $^7\text{Be}$  in this zone, marked by higher mud content. Ponded water, wrack lines, and flattened vegetation after the large 2020 flood were observed in field

visits, suggesting fairly high velocity water from the MR enters the splay interior via Channel 1 (Figure 25) and deposits sediment during very high water events. Proximal sites are flooded infrequently, but are populated with dense vegetation which may aid in fine particle capture and deposition (see Section 6.3 below). Higher observed mud content in the one interior core may be a result of enhanced trapping efficiency due to lower velocity sheet flow as MR river overbanks the levee and spreads out into the splay interior which has dense, mature vegetation, and large areas of ponding/settling.

All of the sandy mudflats (Figure 13) of the FSP splay (vegetated and unvegetated mudflats, distal SAV) appear to be rapidly infilling over inter-annual timescales (see Section 6.1) but the delivery of new sediment, as recorded in  $^7\text{Be}$  deposition rates (Table 2) is variable in space and time. This spatial variability may be due to the presence of flow pathways within this receiving area (not measured in the present study) rather than hydroperiod since all these areas are intertidal on daily timescales. These flow pathways are likely associated with the multiple secondary channels and inlets that enter the area, as well as inlets that tidally exchange water through the remnant marsh fragments that bound Breton Sound. The sediment focusing due to flow pathways and local elevation may be observed in the dominant grain size class for each geomorphic zone and each individual site. For example, Site 29 on the Unvegetated Mudflat had the highest measured deposition of any site (6.5 cm in 2020) across all seasons, the highest clay content (9%) and the smallest D50 (28 $\mu\text{m}$ ). This suggests this area was a lower energy area of sediment focusing with relatively high trapping efficiency of silt and clay. There does not seem to be a significant difference in grain size between vegetated and unvegetated mudflats on the eastern side of the splay (40% and 38% sand contents,

respectively), but the dominance of silt at these sites reflects the silt dominance of the MR source. In contrast, the Distal SAV sites are among the lowest in elevation (Figure 12), and yet have the highest sand contents of any geomorphic zone and the largest D<sub>50</sub> (73  $\mu\text{m}$  on average). Measured deposition in this zone was low, and  $^7\text{Be}$  was only detected twice at these sites (Figure 16 and Table 2). Bulk densities in this zone were low compared to higher elevations, likely due to the rapid deposition of fines and continual inundation which prevents consolidation. While presence of high mud content has generally been associated with areas of high sediment trapping efficiency in MR splays (Esposito et al., 2017), the Distal SAV site characteristics indicate that the rate and character of sediments deposited in these reaches is controlled by other factors in addition to degree of sheltering of the receiving area from Gulf waves and currents, including (1) suspended grain size of the sediment carried in primary crevasse channels from the MR, (2) degree of connectivity and conveyance energy of secondary channels, (3) effects of large storms, and (4) the effects of vegetation on sediment trapping discussed in the next section.

### ***6.3 Vegetative Controls on Sediment Deposition***

The FSP splay follows the expected vegetation community succession that occurs on prograding deltaic splays in the MRD (Johnson et al., 1985; Shaffer et al., 1992; White, 1993; Carle et al., 2014). This succession is associated with sedimentation history, (i.e. mature communities at the higher portion of the splay and younger communities at lower elevations), and is well documented in the literature, particularly for the well-studied Wax Lake bayhead delta (WLD; Bevington and Twilley, 2018; Cahoon et al., 2011; Carle et al., 2015). Dominant species and their associations found at higher

elevations in the FSP and WLD are the same: *Colocasia esculenta*, *Phragmites australis*, *Polygonum punctatum*, *Typha spp.*, *Schoenoplectus spp.*, and *Zizaniopsis milicea* (Twilley et al., 2019). In the WLD and on the Brant's Pass splay associated with the Cubit's Gap crevasse downriver of FSP, vegetation communities are distributed along continuous gradients of chronosequence and elevation (White, 1993; Cahoon et al., 2011; Ma et al., 2018; Bevington and Twilley 2008). Early in the evolution of the Atchafalya Delta, Johnson et al., described discrete vegetation communities, with abrupt transitions between them (1985).

Vegetation zonation is strongly related to sediment surface elevation in MRD wetlands (Bevington et al., 2022). Newly deposited sediment is anchored with root mats and rhizomes. Vegetation accretes sediment via autochthonous organic matter production and the physical trapping of allochthonous organic particulates from the MR (Reed and Cahoon, 1995). In vertically accreting intertidal flats, rapidly colonizing vegetation growth stabilizes loosely consolidated substrate and litter protects sediment from wave attack and reworking. All of these processes aggrade the substrate to an elevation suitable for colonization of distinct vegetation species or communities, and then the trapping and substrate modifying effects of the vegetation exert geomorphic feedbacks on hydroperiod (Larsen, 2019).

Vegetation on the FSP splay shows complex patterns of zonation with communities that often overlap (Fig. 27).

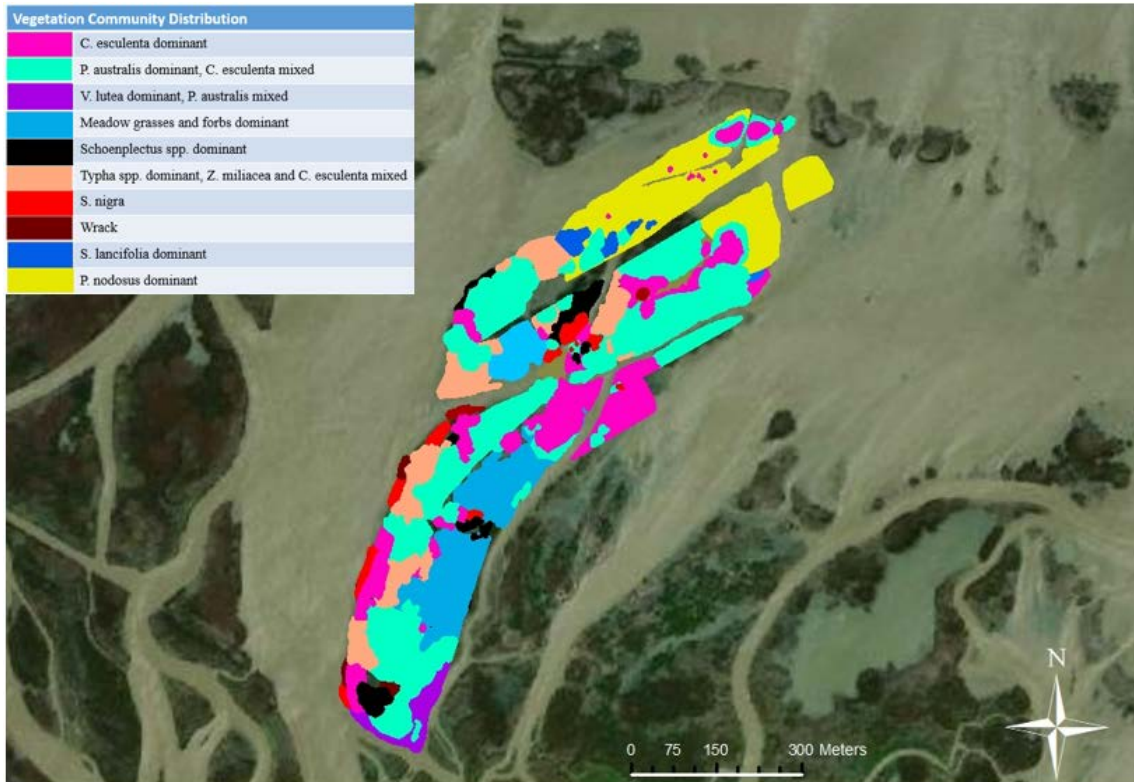


**Figure 27.** Interpretative map of vegetation community distributions constructed using field observations and a high resolution (2 m) drone image of the study site taken in August 2021 (Ramachandran, personal communication).

One instance of this complexity is that the levee zone of the FSP splay has a greater number of distinct patches of vegetation than the interior zone directly on the opposite side, where a continuous meadow of seasonal short grasses and forbs is located. The eastern side of the splay adjacent to Channel 1 is protected by the western natural levee from high velocity MR water, potentially allowing a stable, mature wetland community with higher species diversity to develop (Johnson et al., 1985). The FSP splay has a consistent elevation platform, which averages  $38 \text{ cm} \pm 0.03$  (SE) above MSL, and spans all of the geomorphic zones except the prograding Distal SAV zone. While the marsh elevation of WLD converges toward an equilibrium elevation of 56 cm NAVD88, areas with this elevation are volumetrically clustered towards the up-delta island locations. The

FSP is located in the Birdsfoot Delta which is an area of high subsidence (18.1 – 22.5 mm/yr; Fitzpatrick, 2021). The high and spatially consistent elevation platform in the face of high subsidence may be indicative of the large mineral sediment flux to the island. Stability of marsh on the FSP splay, with its relatively high diversity and evenness, might be linked to the high and consistent mineral flux (supported by high  $^7\text{Be}$ ) that keeps elevation roughly steady through time. As in other MRD splays, monotypic patches with less complex associations tend to be located on the lower elevation mudflats, as the pioneering species that colonize there (*Typha spp.*, *C. esculenta*, *S. lancifolia*, *P. nodosus*) are able to withstand prolonged flooding (Odum, 1969).

Previous studies have shown that vegetation stem density patterns of distribution exert a major control on the magnitude and spatial extent of sediment deposition, (Lenard and Luther 1995; Christiansen, 2000; Temmerman et al., 2004; Nepf, 2012; Kirwan and Megonigal, 2013, Nardin and Edwards, 2014), but the record of these effects on the FSP splay are complicated by the controls discussed in previous sections. For instance, seasonally variable sediment input associated with hydroperiod and MR source (Section 6.2) obscures whether changes in stem density exert a significant control on sediment trapping. The geochronology used in the present study was not definitive in determining if vegetation density and distribution does impact sedimentation. For example, a patch vegetated with a monotypic stand of *C. esculenta* experienced less deposition (2.5 cm deposition in March 2021 coring) than an adjacent bare mudflat (4.5 cm deposition in August 2021 coring). A broader control on sedimentation patterns on the FSP splay are the crevasse primary and secondary channels established around marsh remnants, which confine and focus sediment delivery along pre-existing pathways to some areas more than

others, and determining the role of vegetation within those patterns is difficult. Isolation of the role of aboveground vegetation density on sediment trapping will require measurement of near bed flow and sediment parameters during episodes when the splay is inundated with relatively high velocity, turbid river water from the primary and secondary channels. This was a set of measurements intended for the present study using small-scale stream gaging methods, but these conditions did not occur during any of the 2020 – 2021 surveys.

Wrack deposits on the FSP splay may play an important role in sediment trapping, although they are variable in space and time: predominantly forming after high flow events and during seasons of senescence when stems are more easily detached. Extensive wrack deposits might even become the foundation of an entirely new substrate, further raising the marsh platform as mineral and allocthonous organic riverine inputs collect and accrete within them. Most of this wrack appears to be contributed by *P. australis*, which has heavily lignified standing shoot and rhizome biomass. The significantly higher organic matter content (23% LOI) in the Interior, where stands of *P. australis* proliferate is likely due to the extensive ponding observed in this zone, which causes anoxic soil conditions and slows the decomposition of this recalcitrant wrack. Another impact of vegetation on sediment trapping is that intertidal areas in FSP were observed to be bare in the Winter-Spring period and populated with SAV and extensive floating aquatic vegetation during Summer-Fall. SAV and floating aquatic vegetation may be a major unrecognized trapping effect of vegetation on the leading edge of accreting splays. Although *P. nodosus* and other SAV found in association (*Myriophyllum spicatum* (watermilfoil), *Stuckenia pectinate* (sago pondweed)) appear to play a seasonal role in

slowing water velocities and enhancing the deposition of mineral particles, the  $^7\text{Be}$  data did not definitively show this. Only one Distal SAV site had deposition during the growth season in August (3.5 cm), although deposits enriched in sand sizes do not adsorb  $^7\text{Be}$ . While the role of SAV in sediment trapping has not been well studied, numerical modeling has been used to demonstrate that SAV adds hydraulic resistance to flow, causing a decrease in velocity and maximum bed shear stress to induce mouth-bar formation (Lera, 2019). Ma et al. (2018) found that in the WLD, net positive elevation changes were highest in the lowest parts of the delta that are either open water or SAV dominated (up to 47 mm). In contrast, Beltran (2019) observed lower mineral sediment accumulation rates as mudflat SAV densities increased during summer.

The stem density and stem volume of vegetation growing on the FSP splay, which has been linked to sediment trapping efficiency in marshes in the literature (Morris et al., 2002; Bouma et al., 2009; Mudd et al., 2010; Nardin and Edmonds, 2014) is strongly seasonal and varies by species. This means that each species of vegetation has a season of peak growth which interacts with the hydroperiods discussed in Section 6.2, to enhance deposition and accretion. Figure 20 shows an orders of magnitude (log scale) difference in the barrier to flow in the near-bed region ( $z = 0\text{-}5$  cm) depending on vegetation species. It can be inferred from this that sediment trapping efficiency is highly species specific on the FSP splay. In contrast, there was not an appreciable difference observed in seasonal field studies in 2021, at most sites, between stem densities over the course of the year for individual species (Table 2 in Appendix A). This may be because the present survey focused on near bed stem density, to capture the volume of vegetation at the elevation above the bed that most frequently encounters flow when the splay is

submerged. While vegetation generally increases in height and leaf area over the growing season, there are limited changes in the number of stems per patch and density near the bed (Table 3 in Appendix A).

Surficial grain size characteristics for each geomorphic zone may be an indicator that different vegetation communities on the FSP splay have distinct sediment trapping efficiencies (Figure 15A). Figure 15A shows that there are two modes of grain sizes for all of the dominant species present on the splay: fine sand and silt. The silt mode occurs at  $\sim 40 \mu\text{m}$  and is present in the substrate of all of the dominant vegetation species. *C. esculenta* and *P. australis* substrates tended to have a higher content of fines, potentially indicative of higher trapping efficiency, and no sand. *C. esculenta* and *P. australis* are the two dominant species across the FSP splay and have the highest stem densities across all seasons. *P. nodosus*, which only occurs in the distal SAV zone, has the highest fine sand content out of all the dominant species (Figure 15A). It also has the highest stem densities of any species surveyed, even though it was only observed and measured in August. This high sand content in the SAV substrate either indicates a high seasonal trapping efficiency (large particle trapping), for *P. nodosus* or is related to the character of suspended sediment reaching this intertidal flat (see Section 5.2). Nardin et al., (2016) show that dense and tall vegetation, such as that growing in the proximal and levee zones, can force channelized flow to bypass these areas and carry sediment away to accumulate in the distal region. It is ultimately unclear whether this fine sand was carried in suspension from primary channel, is a result of the process of wave winnowing and reworking of the distal mudflats, or has a distinct offshore origin.

#### ***6.4 Sedimentary Evolution of the FSP Splay***

Sedimentation history, basin geometry, and subsidence control how the FSP study splay will be emplaced in the geologic record of the lower MR delta. The sediments found within the FSP splay are mixtures of very fine sand and silt: coarse distal facies suggest that, as progradation and aggradation continues, the sequence will fine upwards. Crevasse splays are typically preserved in the stratigraphic record as facies with a bottom layer of prodelta clay that coarsens upwards, overlain with a package of interbedded sand and silt that fines upwards (Wilson and Allison, 2008; Bomer et al., 2017; Wang et al., 2019). This silt and sand package is then capped with an organic rich mud facies that is thin and poorly developed due to frequent river flushing (Kosters 1989; Wilson and Allison, 2008). Wang et al. (2019) found that in cores taken distally from the lower Breton Sound, the top three facies were root-rich soft mud, organic rich peat, and massive mud, all of which would be easily eroded during the development of a new crevasse splay. The older, underlying facies were comprised of organic-poor silty sand that act as a firm and less erodible foundation for new land. The FSP splay has already undergone the crevassing event that eroded the top layers of organic rich marsh and revealed the organic-poor (prodelta) silty sand package underneath. Now, those more compacted and resilient facies are being loaded with mineral sediment and abundant sand from the MR, which could provide a more stable substrate for new land. The FSP splay will be emplaced in the stratigraphic record as a package of upward fining coarse sediment that has low organic matter content. The overall high bulk densities, low porosities, and low organic contents in the surficial layers of sediment is evidence that the FSP splay is in its active phase and is receiving high clastic input from the MR. If the FSP crevasses were

allowed to seal, cutting off new sediment supply from the river, as is typical of natural crevasses, the package could be expected to be capped by an organic-rich, marsh poor facies that would eventually subside to open water if organic accumulation rates could not keep pace with local subsidence.

The geometry of the basin in which the FSP study site is located exerts a first – order control on splay morphological evolution. Basins can be enclosed (Davis Pond Freshwater Diversion), semi-enclosed (WLD), or open (Birdsfoot Delta) (Keogh et al., 2019). The FSP splay is located in relatively sheltered and enclosed environment and is bounded by a distal fringe of older, pre-crevasse remnant marsh which provides a barrier from Gulf energy. The prograding edge of the FSP splay contains extensive seasonal SAV and floating aquatic vegetation growth, which further promote sediment retention. Boat examination of the area immediately seaward of the remnant marsh fringe during the 2020-2021 survey showed limited to no areas of SAV/floating vegetation. In contrast, the Wax Lake Delta empties in to a basin that is unprotected from Gulf energy except by the wave-dampening characteristics of a mud blanket in Atchafalaya Bay and the adjacent shelf (Neill and Allison, 2005; Sheremet et al., 2011) . In the Wax Lake Delta, sediments are highly impacted by cold fronts and tidal activity that redistribute sediment on the Gulf shelf (Zhang et al., 2022; Shaw et al., 2013)). The sand, silt, and clay fractions of the surficial sediment in the semi-enclosed basin of West Bay, on average, represent 38.7%, 47.7%, and 13.6% (Xu et al., 2016). The enclosed basin of Big Mar contains 24%, 60.1% and 14.9%. Deposits on the FSP splay contain an average of 46% sand, 50.4% silts, and 3.7% clay, which indicates a significantly high trapping of sand, as discussed above, and a very mineral rich sediment load overall.

Sand is recognized to be the most important material for the growth of a subaerial delta and can provide a more compactionally stable substrate for sediment loading required to build coastal wetland (Roberts et al., 2003; Allison and Meselhe, 2010). Up to 80% of the sand load of the MR and Red River is sequestered upstream, thus it is important to create MR channel diversions that capture sand from suspension to build splay deposits, as is occurring on the FSP splay (Allison and Meselhe, 2010). A key part of the high sediment trapping efficiency of the FSP splay is the Breton Marsh fringe, which provides a seaward boundary that protects the very fine sand and muds delivered via suspension from the MR from redistribution by wind and tidal energy. The Breton Marsh is a natural analog for the sediment retention enhancement devices ('SREDS') that were constructed to promote sediment retention in the West Bay receiving basin by slowing flow velocities within the diversion channel and have been shown to increase sand trapping (Xu et al. 2016; Yuill et al., 2009).

The FSP crevasse complex has been open and receiving MR flow and sediment for about 50 years, which is the span of time that is often used to predict the efficacy of the sediment diversion land building models under development by the state of Louisiana. The evidence of deposition and growth on the FSP splay that has likely accelerated in recent years is supported by a study by White et al. (2019), which used an Integrated Compartment Model (ICM) that has been developed for the state of Louisiana's Coastal Master Plan to model hydrologic, vegetation, and wetland elevation dynamics to determine drivers of wetland change under scenarios of RSL. The White et al. study, which models future land change starting in the year 2015, showed that in the distal region of the FSP complex (beyond the study splay area), land increased in the

future under all of the modeled scenarios except the highest rates of RSLR, and despite reduced inundation due to land aggradation, the FSP marsh surface accreted faster than local RSLR. The model showed that the increase in deposited sediments is gradual during the first two decades, (2015-2035) but increases dramatically by year 30. After the first 20 simulated years, the distal zone slowly shoals into the open water area beyond the Breton Marsh fringe. By year 50 (2065) under the Low RSLR scenario, the entire FSP study splay and surrounding marsh area has infilled, with a large reduction in open water area distally (Figure 28). This land building effect would likely be limited if higher RSLR rates occur in later decades, but based on deposition rates observed in the present study, it is possible that the FSP splay will persist under maximum rates of ESLR (0.83 m/50 yr) and subsidence (3.5 cm/yr) (Reed et al., 2020). These model results provide a time horizon for the infilling observed in the present study to reach completion. However, the importance of (1) a stable sourcing of sediment and water from the MR, (2) the effects of vegetation at a species level on sediment trapping, (3) loading induced subsidence, (4) the continued protection of the evolving splay from direct Gulf wave attack by the degrading remnant Breton Marsh fringe, and (5) climate driven sea level rise, will be important determinants of how land building in FSP will progress in the future. Field studies like the present one can provide information to capture the effects of these processes in more realistic predictive models.

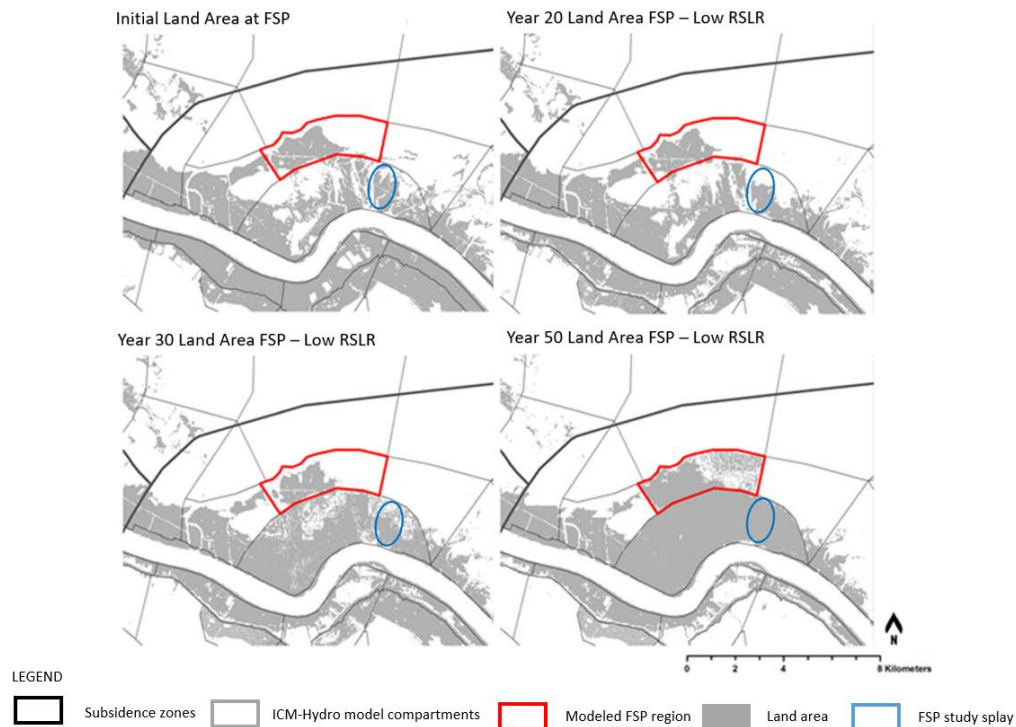


**Figure 28.** Future model projections of land change in the FSP region adapted from White et al. (2019). Maps show progressive land change in the FSP crevasse complex over 50 years under a Low RSLR scenario. FSP study splay is circled in blue.

## 7. CONCLUSIONS

The results of the present study suggest splay elevation (e.g., hydroperiod), proximity to the MR and the crevasses that feed riverine sediment directly to the receiving area, and species level differences in sediment trapping by vegetation are all first-order controls on FSP splay evolution. Specifically:

1. The location of primary and secondary crevasse channels provide pathways that route suspended sediment from the MR to specific areas on the splay. The character of the sediment received on the splay is a function of both the nature of

how sediment is captured from the upper water column of the river and variations in concentration through the channel complex.

2. Hydroperiod is a first-order control on the magnitude and duration of sediment delivery to the splay surface. The splay has an overall pattern of sloping away from the older, proximal sections closer to the river that are ~0.5 m above the prograding distal edge in the intertidal area. Inundation of higher portions of the splay during episodic events is controlled by a combination of (1) coastal setup during winter frontal storms and tropical storms, (2) summer thermal expansion of the Gulf, (3) astronomical tidal conditions, and (4) MR stage. Episodic flooding of the higher-elevation proximal splay can occur in any season. The concentrations of suspended sediment delivered to the splay by the MR is influenced by rising versus falling limb conditions, flood magnitude, and flood duration. The prolonged major flood of 2020 delivered more sediment than the equally high, but shorter duration 2021 flood.
3. The sheltered setting of the FSP splay and distinct receiving area boundary created by the remnant Breton Marsh fringe enhances sediment retention with the FSP crevasse complex. All the sub-tidal elevation areas (sandflats and mudflats) on the FSP splay are infilling over inter-annual timescales. Marsh area on the FSP splay has expanded by an estimated 51 ha since 2006.
4. The FSP vegetated splay deposits are mineral rich (LOI ~6-12%) and also have high contents of fine to very fine sand (28 – 61%) relative to other active splays in the MRD, reflecting the dominant influence of the MR input and the high flow velocities in the crevasse (delivery) channels. Measured rates of <sup>7</sup>Be

geochronology suggest that marsh surfaces on the splay receive several cm/y of sediment, which is a rate that meets or exceeds that of inferred subsidence in the area.

5. Vegetation growth contributes to sediment trapping on the FSP splay through seasonally variable stem densities, and dominant plant species show distinct trapping efficiencies. Each dominant species has a unique life history that maximizes the volume of submerged biomass interacting with flow during all seasons. Wrack deposits in the higher elevation areas and SAV/floating vegetation in the intertidal are seasonal variables which may enhance sediment trapping. Vegetation communities on the FSP splay are similar to those found on other MRD splays and bayhead deltas, but follow complex patterns of zonation that are patchy and often overlap.
6. The FSP crevasses have been opened for 50 years, which is often cited as the lifespan of coastal restoration projects aimed at land-building. For the first ~35 y after the 1973 crevassing, the study area and FSP area overall was net erosional. This pattern of initial erosion of remnant marshes with an influx of high velocity river water has been predicted from artificial large MR sediment diversions authorized by the State of Louisiana. The FSP splay has become an area of net deposition and accelerating marsh growth in the past 14 years. This provides important insight into the timeline and potential subaerial marsh area expansion within receiving basins of future planned river diversions. It may be important to increase the life-span of sediment diversion projects, as the process of land building in this setting acts on geological time scales.

## 8. REFERENCES CITED

Allison, M. A., Chen, Q. J., Couvillion, B., Leadon, M., McCorquodale, A., Meselhe, E. and White, E. D. (2017). Coastal master plan: model improvement plan, attachment C3–2: marsh edge erosion. Coastal Protection and Restoration Authority of Louisiana, 72pp.

Allison, M. A., Demas, C.R., Ebersole, B.A., Kleiss, B.A., Little, C.D., and Meselhe, E.A. (2012). A water and sediment budget for the lower Mississippi-Atchafalaya River in flood years 2008-2010: implications for sediment discharge to the oceans and coastal restoration in Louisiana. *Journal of Hydrology*, 432, 84-97.

Allison, M. A., Sheremet, A., Goñi, M. A., & Stone, G. W. (2005). Storm layer deposition on the Mississippi–Atchafalaya subaqueous delta generated by Hurricane Lili in 2002. *Continental Shelf Research*, 25(18), 2213-2232.

Allison, M.A., and Wilson, C. (2008). An equilibrium profile model for retreating marsh shorelines in southeast Louisiana. *Estuarine, Coastal and Shelf Science*, 80(4), 483-492, doi:10.1016/j.ecss.2008.09.004.

Allen. P.A. (2017). *Sediment routing systems: The fate of sediment from source to sink*. Cambridge University Press. ISBN 978-1-107-09199-3.

Ameen, A.D., Kolker, A.S., Taylor, C.M. (2018). Morphological responses to competition modulated by abiotic factors in two monoculture-forming wetland plants. *Aquatic Botany*, 147, 61-67, <https://doi.org/10.1016/j.aquabot.2018.03.003>.

Amer, R., and Potter, C. (2020). Mapping 30 years of change in the marshlands of Breton Sound basin (Southeastern Louisiana, U.S.A.): coastal land area and vegetation green cover. *Journal of Coastal Research*, 36(3), 437-450.

Amer, R.; Kolker, A., and Muscietta, A. (2017). Propensity for erosion and deposition in a deltaic wetland complex: Implications for river management and coastal restoration. *Remote Sensing of Environment*, 199, 39–50.

Baustian, M.M., Meselhe, E., Jung, H., Sadid, K., Duke-Sylvester, S.M., Visser, J.M., Allison, M.A., Moss, L.C., Ramatchandirane, C., Sebastiaan van Maren, D., Jeuken, M., Bargu, S. (2018). Development of an Integrated Biophysical Model to represent morphological and ecological processes in a changing deltaic and coastal ecosystem. *Environmental Modelling and Software*, 109, 402-419.

Barras, J.A. (2007). Satellite images and aerial photographs of the effects of Hurricanes Katrina and Rita on coastal Louisiana. U.S. Geological Survey, Data Series 281. <http://pubs.usgs.gov/ds/2007/281>, Reston, Virginia.

Beltran, M.B. (2021). Effects of vegetation seasonality on sediment dynamics in a freshwater marsh of the Mississippi River Delta. (M.S. Thesis, Tulane University). Tulane University Theses and Dissertations Archive.

Bevington, A.E., Twilley, R.R., Sasser, C.E. (2022). Deltaic floodplain wetland vegetation dynamics along the sediment surface elevation gradient and in response to disturbance from river flooding and hurricanes in Wax Lake Delta, Louisiana, USA. *Geomorphology*, 398, 108011, <https://doi.org/10.1016/j.geomorph.2021.108011>.

Bevington, A.E., Twilley, R.R. (2018). Island edge morphodynamics along a chronosequence in a prograding deltaic floodplain wetland. *Journal of Coastal Research*, 34(4), 806-817.

Blum, M.D., & Roberts, H.H. (2009). Drowning of the Mississippi Delta due to insufficient sediment supply and global sea – level rise. *Nature Geoscience*, 2(7), 488-491.

Bomer, E.J., Bentley, S.J., Hughes, J.E.T., Wilson, C.A., Crawford, F., & Xu, K. (2019). Deltaic morphodynamics and stratigraphic evolution of Middle Barataria Bay and Middle Breton Sound regions, Louisiana, USA: Implications for river-sediment diversions. *Estuarine Coastal and Shelf Science*, 20-33. doi: [10.1111/j.1600-0706.2008.16892.x](https://doi.org/10.1111/j.1600-0706.2008.16892.x).

Bouma, T.J., Friedrichs, B., van Wesenbeeck, K., Temmerman, S., Grad, G., Herman, P.M.J. (2009). Density-dependent linkage of scale-dependent feedbacks: a flume study on the intertidal macrophyte *Spartina angelica*. *Oikos*, 118, 260-628.

Cahoon, D.R., and Reed, D.J. (1995). Relationships among marsh surface topography, hydroperiod, and soil accretion in a deteriorating Louisiana salt marsh. *Journal of Coastal Research*, 11(2), 357-369.

Cahoon, D.R., White, D.A., Lynch, J.C. (2011). Sediment infilling and wetland formation dynamics in an active crevasse splay of the Mississippi River delta. *Geomorphology*, 131, 57-68.

Coastal Protection and Restoration Authority (CPRA). (2017). Louisiana's Comprehensive Master Plan for a Sustainable Coast. State of Louisiana.

Carle, M.V., Sasser, C.E., & Roberts, H.H. (2015). Accretion and Vegetation Community Change in the Wax Lake Delta Following the Historic 2011 Mississippi River Flood. *Journal of Coastal Research*, 31(3), 569-587.

Carle, M.V., Wang, L., Sasser, C.E. (2014). Mapping freshwater marsh species distributions using WorldView-2 high resolution multispectral satellite imagery.

International Journal of Remote Sensing, 35(13), 4698-4716,

doi:10.1080/01431161.2014.919685

Chen, Z., Ortiz, A., Zong, L., Nepf, H. (2012). The wake structure behind a porous obstruction and its implications for deposition near a finite patch of emergent vegetation.

Water Resources Research, 48, W09517, doi: <https://doi.org/10.1029/2012WR012224>.

Christiansen, T., Wiberg, P.L., Milligan, T.G. (2000). Flow and sediment transport on a tidal salt marsh surface. Estuarine, Coastal and Shelf Science, 50, 315-331,

doi:10.1006/ecss.2000.0548.

Craig, N.J., Turner, R.E., Day, J.W. (1979). Land loss in coastal Louisiana (U.S.A).

Environmental Management, 3(2), 133-144, retrieved from

[https://digitalcommons.lsu.edu/oceanography\\_coastal\\_pubs/166](https://digitalcommons.lsu.edu/oceanography_coastal_pubs/166).

Coleman, J.M. (1988). Dynamic changes and processes in the Mississippi River Delta.

Geological Society of America Bulletin, 100(7), 999-1015.

Coleman, J.M., and Gagliano, S.M. (1964). Cyclic sedimentation in the Mississippi River

deltaic plain. Transactions Gulf Coast Association of Geological Societies, 14, 67-80.

Costanza, K. and Frank-Gilchrist, D. (2019). Summary Report of Supplemental Analysis – Pictorial Accounting of Landscape Evolution of the Crevasses Near Fort St. Philip, Louisiana – 2008 to Present (WBS 9.2.3.15.3). CE Hydro, LLC.

Couvillion, B., Beck, H., Schoolmaster, D., Fischer, M. (2017). Land area change in coastal Louisiana (1932 to 2016). Geological Survey Scientific Investigations Map 3381, 16 pp.

Couvillion, B. and Beck, H. (2013). Marsh collapse thresholds for coastal Louisiana estimated using elevation and vegetation index data. In: Brock, J.C.; Barras, J.A., and Williams, S.J. (eds.), Understanding and Predicting Change in the Coastal Ecosystems of the Northern Gulf of Mexico. Journal of Coastal Research, Special Issue No. 63, pp. 58–67.

Couvillion, B.R., Barras, J.A., Steyer, G.D., Sleavin, W., Fischer, M., Beck, H., and Heckman, D., (2011). Land area change in coastal Louisiana from 1932 to 2010, USGS Scientific Investigations Map No. 3164, 12 pp.

Day, J.W., Kemp, D.J., Reed, D.R., Cahoon, R.M., Boumans, J.M., Suhayda, R. (2011). Vegetation death and rapid loss of surface elevation in two contrasting Mississippi delta salt marshes: the role of sedimentation, autocompaction and sea-level rise. Ecological Engineering, 37(2), 229-240.

Day, J.W., Ibanez, C., Scarton, F., Pont, D., Hensel, P., Day, J., Lane, R. (2011). Sustainability of Mediterranean deltaic lagoon wetlands with sea-level rise: the importance of river input. *Estuaries and Coasts*, 34, 483-493.

Delaune, R.D., Sasser, C.E., Evers-Hebert, E., White, J.R., Roberts, H.H. (2016). Influence of the Wax Lake Delta sediment diversion on aboveground plant productivity and carbon storage in deltaic island and mainland coastal marshes. *Estuarine, Coastal and Shelf Science*, 177, 83-89.

Esposito, C.R., Shen, Z., Tornqvist, T.E., Marshak, J., & White, C. (2017). Efficient retention of mud drives land building on the Mississippi Delta plain. *Earth Surface Dynamics*, 5, 387–397.

Fagherazzi, S., (2013). The ephemeral life of a salt marsh. *Geology*, 41(8):943-944.

Fagherazzi, S., Kirwan, M.L., Mudd, S.M., Guntenspergen, G.R., Temmerman, S., D'Alpaos, A., Clough, J. (2012). Numerical models of salt marsh evolution; Ecological, geomorphic, and climactic factors. *Reviews of Geophysics*, 50(1).

Fauria, K.E., Kerwin, R.E., Nover, D., Schladow, S.G. (2015). Suspended particle capture by synthetic vegetation in a laboratory flume. *Water Resources Research*, 51(11), 9112-9126, <https://doi.org/10.1002/2014WR016481>.

Fisk, H. N. & McFarlan, E. (1954). Sedimentary framework of the modern Mississippi delta. *Journal of Sedimentary Research*, 24(2), 76–99. doi: 10.1306/d4269661-2b26-11d7-8648000102c1865d.

Fitzpatrick, C., Jankowski, K.L., Reed, D. (2021). 2023 Coastal Master Plan: Determining subsidence rates for use in predictive modeling. Coastal Protection and Restoration Authority, Report: Version 1. [www.coastal.la.gov](http://www.coastal.la.gov).

Galler, J.J., and Allison, M.A. (2008). Estuarine controls on fine-grained sediment storage in the Lower Mississippi and Atchafalaya River. *Geological Society of America Bulletin*, 120(3-4), 386-398. doi: <https://doi.org/10.1130/B26060.1>

Hiatt, M., & Passalacqua, P. (2015). Hydrological connectivity in river deltas: The first-order importance of channel-island exchange. *Water Resources Research*, 51, 2264-2282, doi:10.1002/2014WR016149.

Jankowski, K.L., Tornqvist, T.E., Fernandes, A.M. (2017). Vulnerability of Louisiana's coastal wetlands to present-day rates of relative sea-level rise. *Nature Communications*, 8, 14792.

Johnson, W.B., Sasser, C.E., Gosselink, J.G. (1985). Succession of vegetation in an evolving river delta, Atchafalaya Bay, Louisiana. *Journal of Ecology*, 73(3), 973-986.

Keogh, M.E., Kolker, A.S., Snedden, G.A., Renfro, A.A. (2019). Hydrodynamic controls on sediment retention in an emerging diversion-fed delta. *Geomorphology*, 332, 100-111.

Keogh, M.E., Tornqvist, T.E., Kolker, A.S., Erkens, G., Bridgeman, J.G. (2021). Organic matter accretion, shallow subsidence, and river delta sustainability. *Journal of Geophysical Research: Earth Surface*, 126, doi:/10.1029/2021JF006231.

Kolker, A.S., Miner, M.D., Weathers, D.H. (2012). Depositional dynamics in a river diversion receiving basin: The case of the West Bay Mississippi River Diversion. *Estuarine, Coastal and Shelf Science*, 106, 1-12, <https://doi.org/10.1016/j.ecss.2012.04.005>.

Kosters, E. (1989). Organic clastic facies relationships and chronostratigraphy of the Barataria Interlobe Basin, Mississippi Delta Plain. *Louisiana Geological Survey*.

Kirwan, M.L., and Megonigal, P.J. (2013). Tidal wetland stability in the face of human impacts and sea-level rise. *Nature*, 504(7470), 53-60, doi: 10.1038/nature12856.

Lera, S., Nardin, W., Sandford, L., Palinkas, C., Guercio, R. (2019). The impact of submersed aquatic vegetation on the development of river mouth bars. *Earth Surface and Landform Processes*, 44(7), 1494-1506, <https://doi.org/10.1002/esp.4585>.

Larsen, L.G. (2019). Multiscale flow-vegetation-sediment feedbacks in low-gradient landscapes. *Geomorphology*, 334, 165-193.

Leonard, L.A., & Luther, M.E. (1995). Flow hydrodynamics in tidal marsh canopies. *Limnology and Oceanography*, 40(8), 1474-1484.

Ma, H., Larsen, L.G., Wagner, R.W. (2018). Ecogemorphic Feedbacks that Grow Deltas. *Journal of Geophysical Research: Earth Surface*, 123(12), 3228-3250.

Mo, Y., Kearney, M.A., and Turner, R.E. (2020). The resilience of coastal marshes to hurricanes: The potential impact of excess nutrients. *Environment International*, doi: <https://doi.org/10.1016/j.envint.2019.105409>.

Mo, Y., Kearney, M., Momen, B. (2017). Drought- associated phenological changes of coastal marshes in Louisiana. *Ecosphere*, 8(5), <https://doi.org/10.1002/ecs2.1811>.

Morris, J.T., Sundareshwar, P.V., Nietch, C. T., Kjerfve, B., Cahoon, D.R. (2002). Responses of coastal wetlands to rising sea level. *Ecology*, 83(10), 2869-2877, doi: 10.1890/0012-9658(2002)083[2869:ROCWTR]2.0.CO;2.

Mudd, S.M., D'Alpaos, A., Morris, J.T. (2010). How does vegetation affect sedimentation on tidal marshes? Investigating particle capture and hydrodynamic controls on biologically mediated sedimentation. *Journal of Geophysical Research Earth Surface*, 115, 2003–2012, <https://doi.org/10.1029/2009JF001566>.

Nardin, W., Edmonds, D.A., Fagherazzi, S. (2016). Influence of vegetation on spatial patterns of sediment deposition in deltaic islands during flood. *Advances in Water Resources*, 93, 236-248.

Nardin, W. & Edmonds, D.A. (2014). Optimum vegetation height and density for inorganic sedimentation in deltaic marshes. *Nature Geoscience*, doi:10.1038/NGEO2233.

Neill, C.M., and Allison, M.A. (2005). Subaqueous deltaic formation on the Atchafalaya Shelf, Louisiana. *Marine Geology*, 214, 411-430.

Nepf, H.M. (1999). Drag, turbulence, and diffusion in flow through emergent vegetation. *Water Resources Research*, 35, 479-489.

Nepf, H.M. Flow and Transport in Regions with Aquatic Vegetation. (2012). *Annual Review of Fluid Mechanics*, 44, 123-142, doi: 10.1146/annurev-fluid-120710-101048.

Nyman, J.A. (1993). Soil processes related to marsh loss in coastal Louisiana. LSU Historical Dissertations and Theses, 5663,  
[https://digitalcommons.lsu.edu/gradschool\\_disstheses/5663](https://digitalcommons.lsu.edu/gradschool_disstheses/5663).

Nyman, J.A., Walters, R.J., Delaune, R.D., Patrick, W.H. Jr. (2006). Marsh vertical accretion via vegetative growth. *Estuarine Coastal and Shelf Science*, 69, 370-380.

Odum, E.P. (1969). The strategy of ecosystem development. *Science*, 164, 262-270.

Olliver, E.A., & Edmonds, D.A. (2017). Defining ecogeomorphic succession of land building for freshwater, intertidal wetlands in the Wax Lake Delta, Louisiana. *Estuarine, Coastal, and Shelf Science*, 45-57.

Olliver, E.A., Edmonds, D.A., Shaw, J.B. (2020). Influence of floods, tides, and vegetation on sediment retention in the Wax Lake Delta, Louisiana, USA. *JGR Earth Surface*, 125(1), doi: <https://doi.org/10.1029/2019JF005316>

Ortiz, A. C., Roy, S., and Edmonds, D. A., 2017. Land loss by pond expansion on the Mississippi River Delta Plain. *Geophysical Research Letters* 44(8): 3635-3642.

Reed, D., Wang, Y., Meselhe, E., White, E. (2020). Modeling wetland transitions and loss in coastal Louisiana under scenarios of future relative sea level rise. *Geomorphology*, 351, 106991.

Roberts, H.H. (1997). Dynamic Changes of the Holocene Mississippi River Delta Plain: The Delta Cycle. *Journal of Coastal Research*, 13(3), 605-627.

Roy, K.J. (2002) Environmental Assessment: Delta Management at Fort St. Philip (BS-11). U.S. Fish and Wildlife Service. Lafayette, Louisiana. 31 pp.

Sapkota, Y., White, J.R. (2019). Marsh edge erosion and associated carbon dynamics in coastal Louisiana: A proxy for future wetland-dominated coastlines world-wide. *Estuarine, Coastal and Shelf Science*, 226(15), 106289.

Shaffer, G.P., Sasser, C.E., Gosselink, J.G., Rejmanek, M. (1992). Vegetation Dynamics in the Emerging Atchafalaya Delta, Louisiana, USA. *Journal of Ecology*, 80(4), 677-687.

Shaw, J. B., Mohrig, D. and Whitman, S. K. (2013). The morphology and evolution of channels on the Wax Lake Delta, Louisiana, USA. *Journal of Geophysical Research: Earth Surface*, 118(3), 1562–1584.

Shen, Z., Tornqvist, T.E., Mauz, B., Chamberlain, E.L., Nijhuis, A.G., & Sandoval, L. (2015). Episodic overbank deposition as a dominant mechanism of floodplain and delta-plain aggradation. *Geology*, 43(10), 875–878. doi: 10.1130/G36847.1.

Snedden, G., Cable, J.E., Swarzenski, C.M. (2007). Sediment discharge into a subsiding Louisiana deltaic estuary through a Mississippi River diversion. *Estuarine Coastal and Shelf Science*, 71(1), 181-193, doi: 10.1016/j.ecss.2006.06.035.

Suir, G.M., Jones, W.R., Garber, A.L., and Barras, J.A. (2014). Pictorial account and landscape evolution of the crevasses near Ft. St. Philip, Louisiana. *Mississippi River Geology and Potomology Program, Report no. 2, US Army Corps of Engineers Mississippi Valley Division, Vicksburg, MS, 47p.*

Swenson, D. (2019). Mississippi river diversions led to land loss, not growth study says: Implications are ‘obvious’. *Nola.com*, retrieved from

[https://www.nola.com/news/environment/article\\_a1df60ba-c05d-11e9-bf17-d70dd5dd90dc.html](https://www.nola.com/news/environment/article_a1df60ba-c05d-11e9-bf17-d70dd5dd90dc.html)

Temmerman, S., Govers, G., Wartel, S., Meire, P. (2004). Modelling estuarine variations in tidal marsh sedimentation: response to changing sea level and suspended sediment concentrations. *Marine Geology*, 212, 1-19.

Temmerman, S., Bouma, T.J., Van de Koppel, J., Van der Wal, D., De Vrie, M.B., Herman, P.M.J. (2007). Vegetation causes channel erosion in a tidal landscape. *Geology*, 35(7), 631-634. doi: <https://doi.org/10.1130/G23502A.1>.

Tornqvist, T.E., Jankowski, K.L., Li, Y.X., Gonzalez, J.L. (2020). Tipping points of Mississippi Delta marshes due to accelerated sea-level rise. *Science Advances*, 6, DOI:10.1126/sciadv.aaz5512.

Turner, E. R., Layne, M., Mo, Y., & Swenson, E.M. (2019). Net land gain or loss for two Mississippi River diversions: Caernarvon and Davis Pond. *Restoration Ecology* <https://doi.org/10.1111/rec.13024>.

Turner, E.R. and McClenachan, G. (2018). Reversing wetland death from 35,000 cuts: Opportunities to restore Louisiana's dredged canals. *PLoS ONE*, 13(12), <https://doi.org/10.1371/journal.pone.0207717> D

Twilley, R.R., Day, J.W., Bevington, A.E., Castaneda-Moya, E., Christensen, A., Holm, G., Heffner, L.R., Lane, R., Aarons, A., Li, S., Freeman, A., Rovai, A.S. (2019). Ecogeomorphology of coastal deltaic floodplains and estuaries in an active delta: Insights from the Atchafalaya Coastal Basin. *Estuarine, Coastal and Shelf Science*, 227(31), 106341, <https://doi.org/10.1016/j.ecss.2019.106341>.

U.S. Fish and Wildlife Services. (2003). Final Environmental Assessment: Delta management at Fort St. Philip BS-11. Ecological Services, Lafayette, Louisiana, retrieved from <https://www.lacoast.gov/reports/project/3890525~1.pdf>.

Wang, J., Xu, K., Bentley, S.J., White, C., Zhang, X., Lui, H. (2019). Degradation of the plaquemines sub-delta and relative sea-level in eastern Mississippi deltaic coast during late Holocene. *Estuarine, Coastal and Shelf Science*, 227(31), 106344, <https://doi.org/10.1016/j.ecss.2019.106341>.

Weathers, H.D., III. and Allison, M.A. (2016). Patterns of water discharge and sediment flux at the Ostrica-Ft. St. Phillip channel complex during high flow. Presentation at State of the Coast, June, New Orleans.

Wellner, R., Beaubouef, R., Van Wagoner, J., Roberts, H.H. and Sun, T. (2005). Jet-Plume depositional bodies—the primary building blocks of Wax Lake Delta. *Gulf Coast Association of Geological Societies Transactions* 55, 867-909.

Wells, J.T., and Coleman, J.M. (1987). Wetland loss and the subdelta life cycle. *Estuarine, Coastal and Shelf Science*, 25, 111-125.

Wells, J.T. (1996). Subsidence, sea-level rise, and wetland loss in the lower Mississippi River delta. In: Milliman, J.D. and Haq, B.U. (eds.), *Sea-Level Rise and Coastal Subsidence*. The Netherlands: Kluwer, pp 282-311.

Willson, C.A., & Allison, M.A. (2008). An equilibrium profile model for retreating marsh shorelines in southeast Louisiana. *Estuarine, Coastal and Shelf Science*, 80, 483-494.

White, D.A. (1993). Vascular plant community development on mudflats in the Mississippi Riverdelta, Louisiana USA. *Aquatic Botany*, 45, 171-194.

White, E.D., Reed, D.J., Meselhe, E.A. (2019). Modeled Sediment Availability, Deposition, and Decadal Land Change in Coastal Louisiana Marshes under Future Relative Sea Level Rise Scenarios. *Society of Wetland Scientists*, 39, 1233-1248.

Wingenroth, J., Yee, C., Nghiem, J., Larsen, L. (2021). Effects of stem density and Reynolds number on fine sediment interception by emergent vegetation. *Geosciences*, 11(3), 136, doi: <https://doi.org/10.3390/geosciences11030136>

Xu, K., Bentley, S.J. Sr., Robichaux, P., Sha, X., Yang, H. (2016). Implications of Texture and Erodibility for Sediment Retention in Receiving Basins of Coastal Louisiana Diversions. *Water*, 8, 26, doi:10.3390/w8010026

Yang, J., and Nepf, J. (2018). A turbulence-based bed-load transport model for bare and vegetated channels. *Geophysical Research Letters*, 45(10), 428-436, doi: <https://doi.org/10.1029/2018GL079319>.

Yuill, B.T., Ashok, K.K., Pereria, J., Allison, M.A., & Meselhe, E.A. (2016). Morphodynamics of the erosional phase of crevasse-splay evolution and implications for river sediment diversion function. *Geomorphology*, 259, 12-29.

Yuill, B.T., Lavoie, D., Reed, D.J. (2009). Understanding subsidence processes in coastal Louisiana. *Journal of Coastal Research*, 10054, 23-36. doi: <https://doi.org/10.2112/SI54-012.1>.

## 9. APPENDICES

### *Appendix A: Seasonal Vegetation Survey Data*

*Table A1. Geographic coordinates of every site location and their corresponding elevation measured with an RTK. Elevations from 2011 were obtained from the USGS LiDAR image.*

Site Number	Latitude and Longitude	RTK Measured Elevation (m)	LiDAR 2011 Ground Points	Location on Splay
13	29.3768228, -89.4431196	0.539	0.330	Proximal
1	29.3775401, -89.4441658	0.454	0.72	Levee
7	29.377037, -89.4437994	0.453	0.930	Proximal
2	29.3791065, -89.4440583	0.381	0.25	Levee
8.5	29.3788975, -89.4432578	0.332	0.45	Interior
3	29.3810414, -89.4431491	0.295	0.23	Levee
4	29.3837332, -89.4421655	0.295	0.23	Levee
19A	29.3822519, -89.4406409	-0.0628	No Data	Medial Mudflat
19B	29.3821038, -89.4406162	0.290	No Data	Medial Mudflat
6.5	29.3851722, -89.4380473	-0.077	0.166	Distal
12	29.3857038, -89.437129	-0.199	0.296	Distal
18	29.3850192, -89.4368137	-0.0023	0.331	Distal
20	29.38097, -89.43862	No Data	0.462	Medial Mudflat
21	29.377104, -89.441372	No Data	No Data	Levee
22	29.3769444, -89.4413889	No Data	No Data	Levee
23	29.379091, -89.440285	No Data	0.15	Levee
24	29.3791667, -89.4402778	No Data	0.20	Levee
25	29.3805556, -89.4394444	No Data	No Data	Medial Mudflat
26	29.3805556, -89.4397222	No Data	No Data	Medial Mudflat
27	29.382126, -89.438184	No Data	No Data	Distal
28	29.382786, -89.437509	No Data	No Data	Distal
29	29.383631, -89.436576	No Data	No Data	Medial Mudflat

**Table A2.** Average stem density per site during each month surveyed.

Average Stem Density (stems per m <sup>2</sup> )			
Site	March	August	November
13	24	37	15
7	74	26	17
1	33	41	23
2	22	49	33
3	17	37	22
4	29	58	37
8.5	50	No data	24.5
19A	24	54	No data
6.5	No data	36	No data
18	No data	304	No data
12	No data	212	No data

**Table A3. Seasonal Vegetation Survey Data Organized by Species**

Season	Species	Site	Density / m <sup>2</sup>	Average Stem Width (cm)	Average Stem Height (cm)	Average Leaf Width (cm)
November	<i>C. esculenta</i>	13	6	0.8	55	13
		7	36	0.3	23	6
		1	10	0.4	22	7
		2	32	0.7	41	9
		3	0	0	0	0
		19A	No data	No Data	No Data	No Data
		4	54	0.47	55	8
		8.5	24	0.75	62	11
March		13	20	0.9	18	6
		7	0	0	0	0
		1	16	2.4	17	7
		2	6	0.8	16	5
		3	28	2.25	21	5
		19A	24	1.6	28	8
		4	28	2.3	30	6
		8.5	12	2.4	10	3
August		13	20	2.2	150	23
		7	30	0.3	16	10
		1	80	1.8	62	12
		2	22	5	125	25
		3	30	2.6	90	13
		19A	54	5.2	120	27
		4	82	4.1	310	17
		8.5	No Data	No Data	No Data	No Data

November	<i>P. australis</i>	13	60	1	380	2
		7	36	0.7	295	1.3
		1	38	0.3	250	0.92
		2	0	0	0	0
		3	0	0	0	0
		4	20	0.7	300	2
		8.5	36	0.3	275	1.7
March		13	34	0.9	115	2.4
		7	120	0.77	48	1
		1	0	0	0	0
		2	0	0	0	0
		3	18	0.8	96	2.5
		4	30	1.25	46	2
		8.5	122	0.6	150	1.8
August		13	42	0.8	235	2
		7	12	0.96	250	Not Reported
		1	48	0.3	86	Not Reported
		2	0	0	0	Not Reported
		3	0	0	0	Not Reported
		4	34	0.7	220	Not Reported
		8.5	No Data	No Data	No Data	No Data
November	<i>S. lancifolia</i>	13	2	0.5	11	5.5
		7	8	0.5	22	2.2
		1	10	0.2	20	2.3
		2	0	0	0	0
		6.5	No Data	No Data	No Data	No Data
		20	142	1.55	33	Not Reported

March		13	0	0	0	0
		7	0	0	0	0
		1	0	0	0	0
		2	0	0	0	0
		6.5	0	0	0	0
		20	No Data	No Data	No Data	No Data
August		13	0	0	0	0
		7	22	0.8	47.5	7
		1	0	0	0	0
		2	40	3	43.5	4
		6.5	36	0.6	47	0.85
		20	No Data	No Data	No Data	No Data
November	<i>Typha spp.</i>	3	22	1.5	300	2
		8.5	30	0.75	225	1.5
March		3	6	1.6	65	1
		8.5	No Data	No Data	No Data	No Data
August		3	26	7.6	141	Not Reported
		8.5	No Data	No Data	No Data	No Data
November	<i>Z. milacea</i>	2	58	2	140	2.5
March		2	84	9	102	1.7
August		2	50	6	150	3.5
November	<i>Schoenplectus spp.</i>	1	2	0.3	200	N/A
March		1	64	0.35	71	N/A
August		1	24	0.25	116	N/A
August	<i>P. nodosus</i>	18	304	0.0018	No Data	7 (length)
		12	212	0.0018	40 (per stem)	Not Reported
November	<i>Alternanthera phil.</i>	13	8	0.5	No Data	0.2 – 1

		7	26	0.5	No Data	
		1	16	0.5	No Data	
		2	8	0.5	No Data	
		8.5	0	0	No Data	
March		13	26	0.5	No Data	
		7	28	0.3	No Data	
		1	18	0.3	No Data	
		2	10	0.3	No Data	
		8.5	16	0.3	No Data	
August		13	48	0.3	No Data	
		7	32	0.5	No Data	
		1	10	0.3	No Data	
		2	0	0	No Data	
		8.5	0	0	No Data	

**Appendix B: Seasonal Bulk Properties****Table B1.** Bulk properties for sediment cores collected during the March 2021 survey.

March 2021				
Core	Depth	LOI (%)	BD g cm <sup>-3</sup>	Porosity
7	0-5	16	2.13	0.824
	5-10	ND	2.24	0.791
	10-15	ND	2.40	0.707
	15-20	ND	1.98	0.702
13	0-5	9.43	2.75	0.685
	5-10	9.75	2.53	0.661
	10-15	12.23	2.51	0.658
	15-20	10.66	2.09	0.671
1	0-5	9.38	1.36	0.702
	5-10	12.38	1.98	0.695
	10-15	5.38	2.43	0.750
	15-20	ND	1.41	0.756
2	0-5	15.09	1.96	0.640
	5-10	13.70	2.03	0.62
	10-15	7.78	1.96	0.641
	15-20	12.13	1.80	0.703
3	0-5	12.64	2.38	0.748
	5-10	15.83	2.29	0.772
	10-15	6.85	1.99	0.495
	15-20	4.92	1.53	1.021
4	0-5	8.41	2.56	0.680
	5-10	9.266	ND	ND
	10-15	13.52	ND	ND
	15-20	8.78	ND	ND
8.5	0-5	23.5	2.38	0.748
	5-10	11.15	2.29	0.773

	10-15	13.05	1.99	0.627
	15-20	10.57	1.53	0.631 2
19A	0-1	10.95	1.12	0.804
	1-2	10.02	0.87	0.721
	2-3	9.81	0.70	0.689
	3-4	10.67	0.85	0.719
	4-5	ND	0.85	0.757
	5-10	12.76	0.87	0.747
	10-15	11.28	0.88	0.723
	15-20	10.43	0.89	0.710
	20-25	9.53	0.72	0.672
	19B	0-1	13.42	0.91
1-2		13.35	1.04	0.775
2-3		13.47	0.81	0.770
3-4		13.99	0.91	0.769
4-5		ND	1.01	0.767
5-10		13.12	0.84	0.737
10-15		10.67	0.96	0.706
6.5	0-1	5.42	0.80	0.654
	1-2	6.45	0.64	0.628
	2-3	ND	0.63	0.604
	3-4	5.45	0.54	0.560
	4-5	4.27	0.35	0.523
	5-10	3.40	0.34	0.509
	10-15	4.63	0.49	0.549
	15-20	4.99	0.42	0.521
12	0-1	6.49	0.41	0.507
	1-2	6.68	0.81	0.633
	2-3	4.64	0.26	0.484
	3-4	6.47	0.930	0.667
	4-5	ND	0.51	0.592
	5-10	ND	0.59	0.529

	10-15	ND	0.51	0.527
18	0-1	3.68	0.32	0.550
	1-2	3.81	0.42	0.529
	2-3	5.81	0.49	0.571
	3-4	ND	ND	ND
	4-5	3.58	0.31	0.524
	5-10	5.18	0.52	1.056
	10-15	4.66	0.45	1.061

**Table B2.** Bulk properties for sediment cores collected during the August 2021 survey.

August 2021				
Core	Depth	LOI (%)	BD g cm <sup>-3</sup>	Porosity
7	0-1	13.58	0.66	0.738
	1-2	13.12	0.64	0.723
	2-3	16.61	0.41	0.747
	3-4	13.52	0.61	0.735
	4-5	13.39	0.73	0.738
	5-6	13.86	0.83	0.759
13	0-1	5.14	0.38	0.562
	1-2	7.52	0.50	0.614
	2-3	9.32	0.49	0.634
	3-4	8.82	0.52	0.639
	4-5	7.12	0.41	0.627
	6-7	3.78	0.46	0.599
	8-9	6.40	0.54	0.600
	10-11	ND	0.40	0.589
1	0-1	13.20	0.56	0.726
	1-2	13.58	0.53	0.740
	2-3	32.10	0.83	0.767
	3-4	16.31	0.83	0.748
	4-5	ND	0.73	0.725
	6-7	ND	1.08	0.730
2	0-1	9.84	0.81	0.705
	1-2	9.93	0.66	0.701
	2-3	9.29	0.62	0.669

	3-4	2.35	0.59	0.659
	4-5	ND	0.77	0.714
	6-7	ND	0.60	0.713
	8-9	ND	0.59	0.741
3	0-1	9.06	0.41	0.794
	1-2	12.31	0.66	0.735
	2-3	10.06	0.77	0.755
	3-4	9.49	0.60	0.728
	4-5	ND	0.65	0.698
	6-7	ND	0.71	0.717
	8-9	ND	0.73	0.698
4	0-1	8.22	1.11	0.698
	1-2	8.18	0.83	0.693
	2-3	9.35	0.82	0.740
	3-4	9.50	0.66	0.746
	4-5	ND	0.56	0.703
	6-7	ND	0.55	0.679
	8-9	ND	0.69	0.676
19A	0-1	11.04	0.60	0.726
	1-2	10.65	0.60	0.720
	2-3	10.17	0.68	0.692
	3-4	10.47	0.51	0.692
	4-5	11.04	0.72	0.717
	5-10	11.25	1.46	0.740
	10-15	10.88	1.31	0.723
19B	0-1	11.30	0.48	0.814
	1-2	10.64	0.56	0.774
	2-3	10.46	0.57	0.753
	3-4	10.35	0.52	0.742
	4-5	10.09	0.56	0.730
	5-10	8.85	1.34	0.708
	10-15	9.60	1.52	0.716
6.5	0-1	11.26	0.72	0.860
	1-2	5.08	0.39	0.622
	2-3	3.49	0.56	0.546
	3-4	3.88	0.51	0.544
12	0-1	11.64	0.62	0.810
	1-2	11.74	0.70	0.780
	2-3	9.68	0.79	0.744
	3-4	10.12	0.55	0.740
	4-5	9.16	0.69	0.710
	5-10	6.68	0.98	0.617
	10-15	ND	0.90	0.540

	15-20	ND	0.90	0.553
18	0-1	9.68	0.46	0.791
	1-2	8.87	0.43	0.758
	2-3	8.52	0.57	0.734
	3-4	8.06	0.55	0.709
	4-5	5.68	0.83	0.628

**Table B3.** Bulk properties for cores collected during the November 2021 survey.

November				
Core	Depth	LOI (%)	BD g cm <sup>-3</sup>	Porosity
2	0-1	10.80	0.84	0.814
	1-2	No Data	1.04	0.768
	2-3	8.25	0.72	0.726
	3-4	No Data	0.86	0.762
	4-5	14.82	0.66	0.820
3	0-1	7.28	0.83	0.754
	1-2	No Data	0.78	0.732
	2-3	7.072	0.58	0.692
	3-4	No Data	0.71	0.672
	4-5	6.556	0.58	0.689
	6-7	No Data	0.52	0.689
	8-9	No Data	0.68	0.722
	10-11	No Data	0.84	0.715
	12-13	No Data	0.66	0.675
	14-15	No Data	0.54	0.692
	15-20	No Data	1.12	0.668
19B	0-1	7.90	1.2	0.857
	1-2	7.92	0.78	0.698
	2-3	8.20	0.85	0.810
	3-4	7.26	0.77	0.758
	4-5	7.38	0.62	0.724
	6-7	6.78	0.65	0.698
	8-9	6.32	1.61	0.859
	10-11	No Data	0.34	0.580
6.5	0-1	5.65	0.69	0.86
	1-2	No Data	0.76	0.622

	2-3	4.11	0.39	0.546
	3-4	3.74	0.70	0.544
12	0-1	6.95	0.63	0.732
	1-2	No Data	0.76	0.704
	2-3	7.55	0.37	0.705
	3-4	No Data	0.53	0.701
	4-5	4.59	0.44	0.572
	6-7	No Data	0.44	0.503
	8-9	No Data	0.36	0.500

### *Appendix C: Grain Size Statistics*

*Table C1. Sediment statistics calculated with GRADISTAT version 9 according to Folk and Ward Method (units of microns).*

Site	Mode1 ( $\mu\text{m}$ ):	Mode2 ( $\mu\text{m}$ ):	Mode3 ( $\mu\text{m}$ ):	Kurtosis	Skewness ( $S\bar{k}_G$ ):
13	37.7	None	None	0.961	0.218
1	104.6	135.5	None	1.049	0.094
7	19.95	15.45	104.6	0.852	0.070
2	153.5	104.6	198.5	0.899	0.138
8.5	81.2	19.95	15.45	0.893	0.095
3	153.5	104.6	None	0.907	0.209
4	48.7	None	None	1.098	0.066
19A	25.75	15.45	104.6	0.071	0.071
20	104.6	135.5	None	0.992	0.178
19B	153.5	198.5	104.6	0.829	0.213
6.5	104.6	None	None	1.146	0.247
12	153.5	104.6	None	1.007	0.271
18	135.5	104.6	None	1.051	0.346
25	92.25	None	None	1.010	0.293
29	29.25	0.721	None	1.171	0.130

**Table C2.** Sediment statistics Using Folk and Ward descriptions and graphic Mean.

Site	Sediment Type	D <sub>10</sub> (µm):	D <sub>50</sub> (µm):	D <sub>90</sub> (µm):	Mean (M <sub>G</sub> ):
13	Very Fine Sandy Very Coarse Silt	8	37	130	35.3
1	Very Coarse Silty Very Fine Sand	12.6	80.6	270	69.4
7	Very Fine Sandy Coarse Silt	5.6	32	179	32.8
2	Very Coarse Silty Fine Sand	9.8	68.7	304	63
8.5	Very Fine Sandy Very Coarse Silt	6	44.8	227	40
3	Very Coarse Silty Fine Sand	11	81.4	307	69.58
4	Very Fine Sandy Very Coarse Silt	12.4	49.6	170	48.8
19A	Very Fine Sandy Coarse Silt	6	33.3	239	36.4
20	Very Fine Sandy Very Coarse Silt	9	49	186	54.8
19B	Very Coarse Silty Fine Sand	7.5	73.3	320	60.5
6.5	Very Coarse Silty Fine Sand	13	70	191	61.4
12	Very Coarse Silty Fine Sand	14.8	86	241	73.2
18	Very Coarse Silty Fine Sand	15	91.5	225	74.2
25	Very Coarse Silt	5.2	44.4	144	36.1
29	Very Fine Sandy Coarse Silt	4	27.8	136.6	26.26

**Table C3.** Fraction of fine size classes found at each site, calculated with GRADISTAT version 9.

Sediment Fraction	1	13	7	8.5	3	4	2	20	19A	19B	6.5	12	18	25	29
% SAND:	57.8%	30.6%	34.3%	41.1%	56.9%	40.7%	52.4%	49.1%	34.8%	53.3%	54.8%	60.2%	63.2%	39%	26%
% MUD:	42.2%	69.4%	65.7%	58.9%	43.1%	59.3%	47.6%	50.9%	65.2%	46.7%	45.2%	39.8%	36.8%	61%	74%
% COARSE SAND:	11.9%	2.8%	5.4%	8.7%	15.1%	4.6%	14.5%	6.9%	9.3%	16.3%	5.1%	9.0%	7.1%	0	0
% MEDIUM SAND:	22.7%	7.9%	12.6%	12.8%	21.7%	12.3%	19.4%	18.9%	12.1%	20.5%	19.1%	26.3%	28.6%	1.7%	3.4%
% FINE SAND:	23.2%	19.9%	16.2%	19.7%	20.1%	23.7%	18.5%	23.3%	13.4%	16.5%	30.6%	24.9%	27.6%	12.3%	8%
% V FINE SAND:	16.9%	26.0%	16.5%	17.4%	15.5%	27.4%	17.0%	20.6%	17.0%	13.4%	21.9%	17.6%	15.7%	25%	14.6%
% V COARSE SILT:	12.6%	21.8%	18.6%	15.1%	13.0%	18.7%	14.4%	14.7%	19.6%	13.2%	11.5%	11.5%	10.6%	20.7%	20%
% COARSE SILT:	7.0%	11.7%	15.0%	12.7%	7.8%	7.5%	8.5%	8.0%	14.4%	9.6%	5.8%	5.4%	5.3%	15.6%	21.8%
% MEDIUM SILT:	3.9%	6.7%	10.3%	9.5%	4.6%	4.1%	5.2%	4.3%	9.4%	6.8%	4.1%	3.5%	3.5%	10.6%	14%
% FINE SILT:	3.9%	6.7%	10.3%	9.5%	4.6%	4.1%	5.2%	4.3%	9.4%	6.8%	4.1%	3.5%	3.5%	6.6%	8.6%
% CLAY:	1.8%	3.2%	5.3%	4.1%	2.1%	1.7%	2.5%	3.3%	4.7%	3.7%	1.9%	1.7%	1.7%	7.5%	9.7%

**Appendix D: <sup>7</sup>Be Depth of Penetration and Activities****Table D1: June 2020 Be7 activities for all cores and intervals.**

June 2020			
Core	Depth (cm)	Activity (dpm/g)	Error ±
21	0-1	3.38	0.48
	1-2	3.61	0.63
	2-3	3.85	0.44
	3-4	1.77	0.29
22	0-1	2.93	0.88
	1-2	1.75	0.52
	2-3	2.19	0.87
	3-4	0	0
23	0-1	1.05	0.19
	1-2	1.08	0.32
	2-3	0.91	0.36
	3-4	0.79	0.27
	4-5	0.86	0.29
	6-7	0.67	0.28
	8-9	0.56	0.31
24	0-1	2.9	0.44
	1-2	2.9	0.35
	2-3	1.8	0.37
	3-4	2.7	0.57
	4-5	0.57	0.3

	6-7	0	0
25	1-2	1.51	0.44
	2-3	0.46	0.65
	3-4	0.57	0.51
	4-5	0	0
26	0-1	0.86	0.25
	1-2	0.89	0.34
27	0-1	1.92	0.58
	1-2	2.54	0.52
	2-3	1.82	0.31
	3-4	1.5	0.38
	4-5	0	0
28	0-1	3.54	0.48
	1-2	4.02	0.58
	2-3	3.93	0.62
	3-4	2.26	0.57
	4-5	0.42	0.51
	6-7	0.53	0.47
29	0-1	3.38	0.45
	1-2	3.47	0.39
	2-3	4.55	0.69
	3-4	4.25	0.67
	6-7	1.05	0.45
	8-9	0.62	0.53

**Table D2.** March 2021 sediment core  $Be^7$  activities over all intervals.

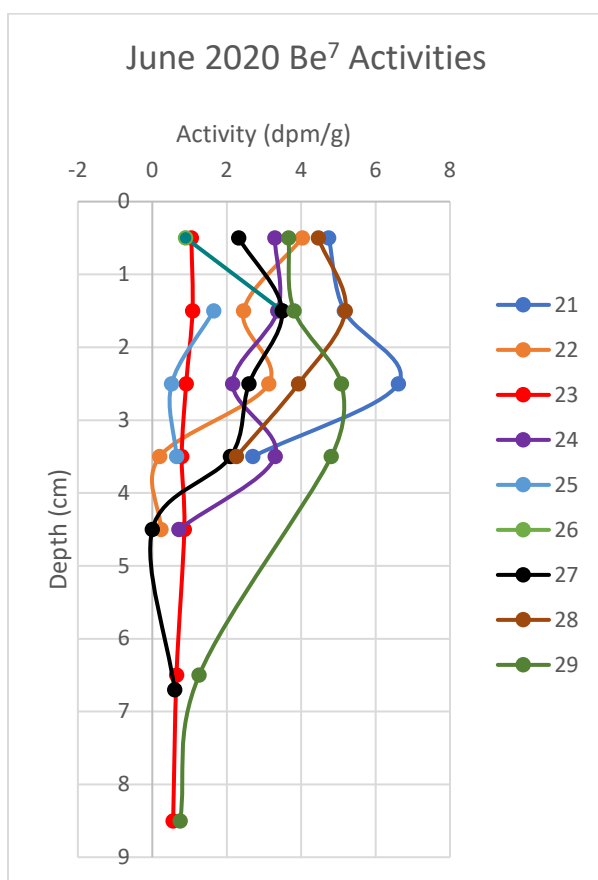
March 2021			
Core	Depth (cm)	Activity (dpm/g)	Error $\pm$
12	1-2	2.42	1.04
19B	1-2	1.39	0.88
	2-3	0.69	0.85
6.5	0-1	1.08	0.60
	1-2	0.34	0.58
	2-3	0.35	0.53
	3-4	0	0
19A	0-1	1.32	1.07
	1-2	1.11	0.81
	2-3	1.29	1.00
	3-4	0	0

**Table D3.** August 2021 sediment core  $Be^7$  activities over all intervals.

August 2021			
Core	Depth (cm)	Activity (dpm/g)	Error $\pm$
7	0-1	0.81	0.74
	3-4	1.26	0.57
	4-5	0.77	0.86
3	4-5	0.56	0.68
13	1-2	1.55	0.52
2	4-5	1.56	0.53
18	3-4	1.51	0.31
4	6-7	0.78	0.82

**Table D4.** November 2021 sediment core  $Be^7$  activities over all intervals.

November 2021			
Core	Depth (cm)	Activity (dpm/g)	Error $\pm$
20	4-5	1.07	0.35
2	4-5	0.21	0.30
2	6-7	0.94	0.45
19B	4-5	2.69	1.08
6.5	4-5	0.47	0.50

**Figure D1.** Downcore 7-Berilyum activities in (dpm/g) for all June 2020 cores.

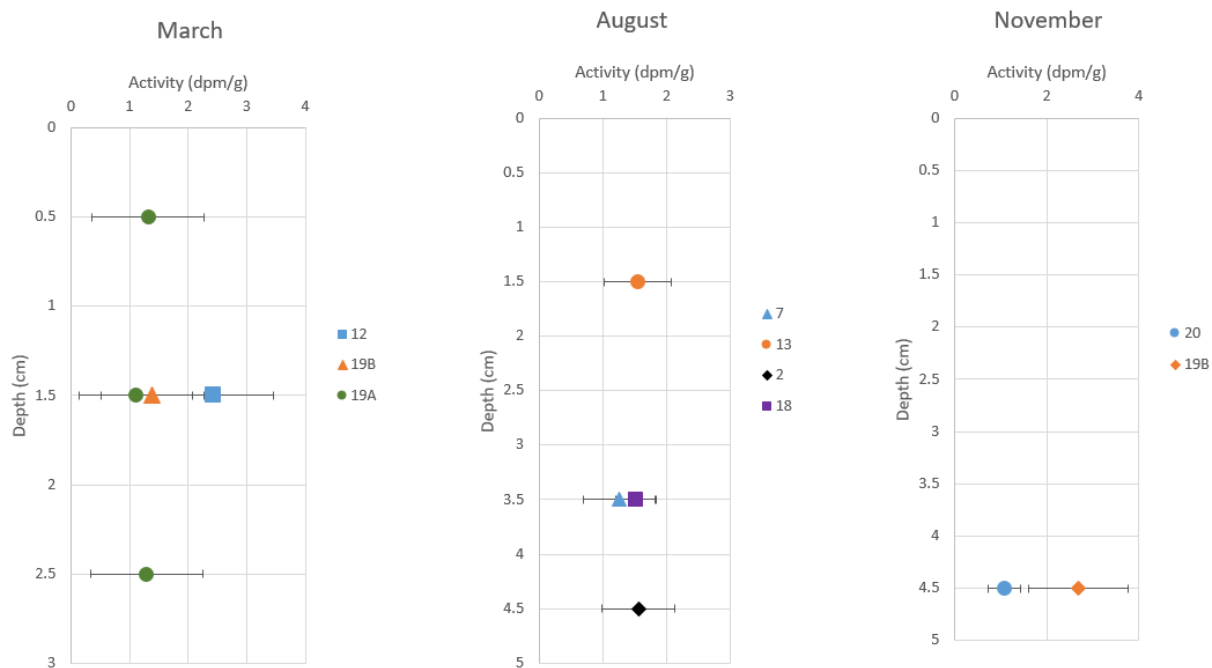


**Figure D2.** Downcore 7-Beryllium activities for all cores over the 2021 survey year.

## BIOGRAPHY

Katrina grew up in Philadelphia and later moved to the San Francisco Bay Area, where she developed a curiosity about ecological restoration and obtained her B.S. in Conservation and Resource Studies from the University of California, Berkeley in 2017. She began an M.S. program at Tulane in 2019, with a focus on River Science and Engineering, under the mentorship of Mead Allison. Katrina intends to remain in New Orleans following graduation to work for the USACE.